Adaptive Target Detection with Polarimetric FDA-MIMO Radar

Lan Lan, *Member, IEEE*, Massimo Rosamilia, *Student Member, IEEE*, Augusto Aubry, *Senior Member, IEEE*, Antonio De Maio, *Fellow, IEEE*, Guisheng Liao, *Senior Member, IEEE*, Jingwei Xu, *Member, IEEE*

***Abstract*—The problem of adaptive radar detection with a polarimetric Frequency Diverse Array Multiple-Input Multiple-Output (FDA-MIMO) radar is addressed in this paper. At the design stage, the target detection problem is formulated as a composite hypothesis test, with the unknowns given by the target angle, incremental range (target displacement with respect to the center of the occupied range cell), and scattering matrix, as well as the interference covariance matrix. The formulated detection problem is handled by resorting to sub-optimal design strategies based on the Generalized Likelihood Ratio (GLR) criterion. The resulting detectors demand, under the H_1 hypothesis, the solution of a box-constrained optimization problem for which several iterative techniques, i.e., the Linearized Array Manifold (LAM), the Gradient Projection Method (GPM), and the Coordinate Descent (CD) algorithms, are exploited. At the analysis stage, the performance of the proposed architectures, which ensure the bounded CFAR property, is evaluated via Monte Carlo simulations and compared with the benchmarks in both white and colored disturbance.**

***Index Terms*—Polarimetric FDA-MIMO radar, target detection, array manifold linearization, coordinate descent algorithm, gradient projection method.**

I. Introduction

In recent decades, the detection of point-like targets exploiting polarimetric diversity techniques has been a popular and extensively studied topic [1–7]. This interest is motivated by the observation that multi-polarimetric measurements might enhance the detection performance of the conventional pulse-Doppler radars in challenging conditions where Doppler discrimination is problematic. This is the case of Doppler ambiguous targets, or targets that move slowly or tangentially and are masked by the clutter environment. In [8], two adaptive detectors based on the Generalized Likelihood Ratio Test (GLRT) and the Wald test, respectively, accounting for the presence of Gaussian clutter with unknown covariance matrix, are derived by capitalizing on the polarization diversity and the spillover of the target energy in consecutive range samples. In [9], the target detection problem is addressed in the context of compound-Gaussian clutter with an unknown covariance matrix, highlighting some interesting and promising improvements on the detectability of small and slowly moving targets in heavy heterogeneous clutter. Remarkably, the derived detector ensures the Constant False Alarm Rate (CFAR) property with respect to (w.r.t.) the texture statistics [9]. Usually, in the open literature, the design of detectors exploiting the polarimetric domain has been mainly focused on traditional single channel radars, phased array radars, and Multiple-Input Multiple-Output (MIMO) architectures [5, 8, 10–13].

Due to the range-angle-dependent beampattern, achieved via appropriate frequency shifts across the transmit antenna elements [14–16], the Frequency Diverse Array (FDA)-MIMO radar has recently received considerable interest from the radar community [16–19]. This configuration provides several benefits, such as the robustness to suppression of mainlobe deceptive jammers [20], as well as improved multipath mitigation performance compared with conventional MIMO systems [17]. As a matter of fact, the joint estimation of angle and range has been widely investigated in FDA-MIMO with different array configurations [21, 22], via the Maximum Likelihood (ML) method [18, 23], compressive sensing approaches [24], the Estimation of Signal Parameters via Rational Invariance Techniques (ESPRIT) [25], and the Multiple Signal Classification (MUSIC) algorithm [26]. As to the detection task, the assessment of the performance for a FDA-MIMO radar has been analyzed in [27], assuming perfect knowledge of target range and angle, as well as the interference covariance matrix. Besides, in [28], the moving target detection problem has been investigated with a FDA-MIMO radar operating in a background of unknown Gaussian interference without any requirement of training data.

Some attempts to extend the plain FDA-MIMO architecture to incorporate polarimetric information have been also pursued in the open literature [29–31], using arrays of dual polarized antennas. In [29], the estimation of the target parameters, i.e., angle, range, and scattering matrix, is accomplished via the ESPRIT algorithm. Moreover, a sparse polarization sensitive FDA-MIMO radar is introduced in [30], exploiting co-prime frequency offsets to improve the range resolution without affecting the maximum unambiguous range. To the best of the authors' knowledge, the target detection problem with a polarimetric FDA-MIMO radar has only received a limited attention. This motivates the study presented in this paper, where the synthesis of adaptive detectors accounting for a disturbance covariance matrix with unknown spectral characteristics, is investigated. At the design stage, the target

The work of L. Lan, G Liao, and J. Xu was supported in part by the National Nature Science Foundation of China (62101402, 61931016, 62071344), China Postdoctoral Science Foundation (2021TQ0261, 2021M702547), and Young Elite Scientists Sponsorship Program by CAST (No. 2021QNRC001).

L. Lan, G Liao, and J. Xu are with the National Key Laboratory of Radar Signal Processing, Xidian University, Xi'an 710071, China. (e-mail: lanlan@xidian.edu.cn, liaogs@xidian.edu.cn; xujingwei1987@163.com).

M. Rosamilia, A. Aubry, and A. De Maio are with the Department of Electrical Engineering and Information Technology, University of Naples "Federico II", I-80125 Naples, Italy, and also with the National Inter-University Consortium for Telecommunications, 43124 Parma, Italy (e-mail: massimo.rosamilia@unina.it; augusto.aubry@unina.it; ademaio@unina.it). (Corresponding author: Antonio De Maio.)

detection problem is formulated as a binary hypothesis test, where the target parameters, i.e., angle, incremental range within the radar cell [23, 32], and scattering matrix, along with the interference covariance matrix, are assumed unknown. Since a Uniformly Most Powerful (UMP) test cannot be derived, some sub-optimal detection architectures based on the GLRT and Two-Step GLRT (2SGLRT) criteria are proposed. Their implementation demands the solution of an optimization problem involving the concentrated log-likelihood functions under the target presence hypothesis. To come up with some practical detectors, the problem at hand is tackled in a sub-optimal but effective way by means of three specific solution techniques:

- the Linearized Array Manifold (LAM) method [33], which solves an equivalent optimization problem leveraging a tailored linearization procedure to represent the target steering vector as the superposition of the pointing direction term plus two contributions that account for the actual angle and incremental range offsets w.r.t. the nominal array steering;
- the Gradient Projection Method (GPM) [34], which iteratively updates the unknown target location parameters, in the concentrated log-likelihood function under the alternative hypothesis, along the current ascent direction (using either a constant stepsize or an adaptive one via the backtracking procedure) from an initial guess until a stationary point is reached;
- the Coordinate Descent (CD) procedure [35], composed of an alternating sequence of one-dimensional (1-D) searches (conducted over discretized intervals) w.r.t. one target location parameter (either angle or incremental range) while keeping the other fixed.

Besides, the bounded CFAR property as well as the computational complexity of the aforementioned GLRT-based detectors are discussed. At the analysis stage, their detection performance is compared with both benchmark and mismatched receivers, which exploit the true and nominal target location parameters, respectively, in white noise and clutter (mixed or trees) environment. The results highlight that the proposed radar architectures can achieve a better probability of detection (P_d) than the counterparts (also including the single polarization receiver), representing viable solutions for practical implementations.

The paper is organized as follows. The signal model for the polarimetric FDA-MIMO radar is presented in Section II. In Section III, the detection problem for a polarimetric FDA-MIMO radar is formulated. Section IV investigates optimization strategies for the computation of GLRT-based detectors and studies the bounded CFARness as well as the computational complexity of the derived algorithms. The performance analysis is addressed in Section V, whereas conclusions are drawn in Section VI.

Notations: Boldface is used for vectors $\boldsymbol{x}$ (lower case), whose n-th entry is $x(n)$, and matrices $\boldsymbol{A}$ (upper case), whose entry in the m-th row and the n-th column is $A_{m,n}$. The transpose, the conjugate, and the conjugate transpose operators are denoted by the symbols $(\cdot)^{\mathrm{T}}$, $(\cdot)^*$, and $(\cdot)^\dagger$, respectively. $\mathrm{diag}(\boldsymbol{x})$ indicates the diagonal matrix whose i-th diagonal element is the i-th entry of $\boldsymbol{x}$. $\boldsymbol{I}$ and $\boldsymbol{0}$ denote respectively the identity matrix and the matrix with zero entries (their size is determined from the context). $\mathbb{C}^N$, $\mathbb{R}^N$, $\mathbb{C}^{N\times M}$ and $\mathbb{H}^N$ are respectively the sets of N-dimensional vectors of complex numbers, N-dimensional vectors real numbers, $N \times M$ complex matrices, and $N \times N$ Hermitian matrices. For any $\boldsymbol{A} \in \mathbb{H}^N$, $\boldsymbol{A} \succeq 0$ means that $\boldsymbol{A}$ is a positive semidefinite matrix. The determinant and the trace of the matrix $\boldsymbol{A} \in \mathbb{C}^{N\times N}$ are indicated respectively with $\det(\boldsymbol{A})$ and $\mathrm{tr}(\boldsymbol{A})$. For any $\boldsymbol{x} \in \mathbb{C}^N$, $\|\boldsymbol{x}\|$ denotes its Euclidian norm, whereas the spectral norm of a matrix $\boldsymbol{A}$ is indicated as $\|\boldsymbol{A}\|$. $\odot$ and $\otimes$ represent the Hadamard (element-wise) product and the Kronecker product, respectively. The letter j indicates the imaginary unit (i.e. $j = \sqrt{-1}$). For any complex number z, $\Re(z)$, $\Im(z)$, and $|z|$ are used to denote the real part, imaginary part, and the modulus of z, respectively. $[a, b]$ indicates a closed interval of $\mathbb{R}$. For any real number y, the function $\mathrm{sign}(y) = -1$ if $y < 0$ and 1 if $y \geq 0$. Besides, $\nabla_{\boldsymbol{x}}[f(\cdot)]$ denotes the gradient of $f(\cdot)$ with respect to $\boldsymbol{x}$, with the partial derivatives arranged in a column vector. C^2 indicates the class of functions with continuous second-order derivatives, whereas $C_L^{1,1}$ denotes the class of functions with Lipschitz gradient with constant L. Finally, $\mathbb{E}[\cdot]$ denotes the statistical expectation.

II. Signal Model For Polarimetric FDA-MIMO Radar

Let us consider a colocated FDA-MIMO radar consisting of M transmit and N receive pairs of crossed dipoles, which are placed in a uniform linear array configuration for both transmission and reception on the xy-plane with array's inter-element spacing equal to d (see Fig. 1). An elliptical electromagnetic polarization for both the transmitted and received signals [36] is considered. It is also assumed that a point-like target is located in the far-field at the angle θ_t and range R_t in the yz-plane.

For the FDA configuration, a frequency increment Δf is introduced at each crossed dipole composing the transmit array, with the first one being the reference. As a consequence, the carrier frequency at the m-th ($m = 1, \ldots, M$) transmitting crossed dipole is [32]

$$f_m = f_0 + (m-1)\Delta f, \quad m = 1, 2, \ldots, M, \tag{1}$$

where f_0 indicates the reference carrier. Besides, each element transmits a specific base-band phase-modulated pulse composed of P subpulses. The resulting complex envelope of the Radio Frequency (RF) signal radiated by the m-th crossed dipole can be expressed as

$$s_m(t) = \sqrt{\frac{E_t}{P}} x_m(t) e^{j2\pi f_m t}, \quad 0 \leq t \leq T_p, \tag{2}$$

with E_t the transmitted energy, T_p the radar pulse duration, and

$$x_m(t) = \frac{1}{\sqrt{\tau_b}} \sum_{p=1}^{P} \varphi_m(p)\, u\left[\frac{t-(p-1)\tau_b}{\tau_b}\right], \quad m = 1, \ldots, M, \tag{3}$$

This article has been accepted for publication in IEEE Transactions on Aerospace and Electronic Systems. This is the author's version which has not been fully edited and content may change prior to final publication. Citation information: DOI 10.1109/TAES.2022.3210887

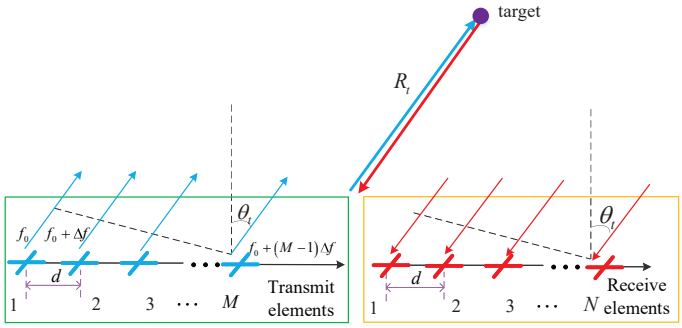

Fig. 1: Illustration of the polarimetric FDA-MIMO radar system.

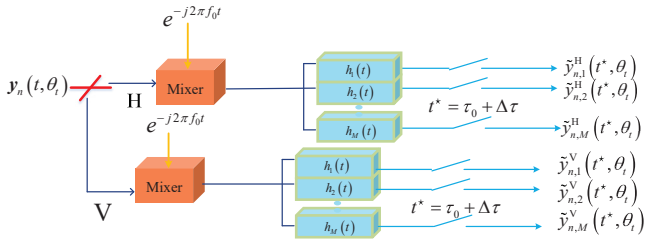

Fig. 2: Signal processing chain at the n-th polarimetric receiver with multiple match-filters.

where $\tau_b = \frac{T_p}{P}$, $u(t)$ is the asymmetric rect function, i.e., $u(t) = 1$ as long as $0 \leq t \leq 1$ and zero elsewhere, and $\varphi_m(p) = e^{j\phi_m(p)}$, with $\phi_m(p) \in [0, 2\pi]$ the p-th entry of the phase code on the m-th transmit array element.

A. Received Signal for Polarimetric FDA-MIMO radar

Let us consider the far-field target having a constant polarimetric scattering matrix $\boldsymbol{\Sigma}_t = \begin{bmatrix} \Sigma_{\mathrm{HH}} & \Sigma_{\mathrm{VH}} \\ \Sigma_{\mathrm{HV}} & \Sigma_{\mathrm{VV}} \end{bmatrix} \in \mathbb{C}^{2\times 2}$ over the FDA-MIMO radar bandwidth, with $\Sigma_{\mathrm{rt}}, \mathrm{r}, \mathrm{t} \in \{\mathrm{H}, \mathrm{V}\}$ the complex target scattering amplitude assuming a polarization 't' on transmit and a polarization 'r' on receive[1].

As shown in Fig. 2, the H and V components received on the n-th polarimetric-spatial channel, i.e., $\boldsymbol{y}_n(t,\theta_t) = \left[y_n^{\mathrm{H}}(t,\theta_t), y_n^{\mathrm{V}}(t,\theta_t)\right]^{\mathrm{T}} \in \mathbb{C}^2, n = 1,\ldots,N$, are firstly multiplied by $e^{-j2\pi f_0 t}$, and then processed through a bank of M matched filters $h_l(t) = x_l^*(-t)\, e^{j2\pi\Delta f(l-1)t}$ $(l = 1,\ldots,M)$. Moreover, after sampling at the range gate of interest and under some mild technical conditions (see Appendix A of [32] for the single polarization case), the received polarimetric signal from the target can be expressed as a $2MN \times 1$-dimensional vector[2]

$$\begin{aligned}\boldsymbol{y}_{\mathrm{S}}(\theta_t,\Delta\tau) = &\left[\tilde{\boldsymbol{y}}_{1,1}^{\mathrm{T}}(t^\star,\theta_t),\ldots,\tilde{\boldsymbol{y}}_{1,M}^{\mathrm{T}}(t^\star,\theta_t),\ldots,\right.\\ &\left.\tilde{\boldsymbol{y}}_{N,1}^{\mathrm{T}}(t^\star,\theta_t),\ldots,\tilde{\boldsymbol{y}}_{N,M}^{\mathrm{T}}(t^\star,\theta_t)\right]^{\mathrm{T}}\\ &= \boldsymbol{\alpha}\otimes(\boldsymbol{b}(\theta_t)\otimes[\boldsymbol{c}(\theta_t)\odot\boldsymbol{a}(\Delta\tau)])\\ &= \boldsymbol{\alpha}\otimes\boldsymbol{s}(\theta_t,\Delta\tau),\end{aligned} \tag{4}$$

where[3]

- $t^\star = \tau_0 + \Delta\tau$ denotes the time instant when the data from the CUT are collected, with $\Delta\tau$ the unknown incremental delay w.r.t. the sampling time associated with the target range cell [32] and $\tau_0 = \frac{2R_t}{c}$ the envelope time delay, respectively;
- $\tilde{\boldsymbol{y}}_{n,l}(t^\star,\theta_t) = \left[\tilde{y}_{n,l}^{\mathrm{H}}(t^\star,\theta_t), \tilde{y}_{n,l}^{\mathrm{V}}(t^\star,\theta_t)\right]^{\mathrm{T}} \in \mathbb{C}^2, l = 1,\ldots,M, n = 1,\ldots,N$, is obtained by filtering the output of the n-th polarimetric channels (after multiplication by $e^{-j2\pi f_0 t}$) with the l-th matched filter and sampling the resulting signal in the Cell Under Test (CUT);
- $\boldsymbol{\alpha} = \boldsymbol{\Sigma}_t \boldsymbol{e}\sqrt{(E_t/P)} \in \mathbb{C}^2$;
- $\boldsymbol{e} = [E_{\mathrm{H}}, E_{\mathrm{V}}]^{\mathrm{T}} \in \mathbb{C}^2$, with E_{H} and E_{V} the horizontal and vertical components of the electric field impinging on the target, respectively;
- $\boldsymbol{s}(\theta_t,\Delta\tau) = \boldsymbol{b}(\theta_t)\otimes[\boldsymbol{c}(\theta_t)\odot\boldsymbol{a}(\Delta\tau)] \in \mathbb{C}^{MN}$ the transmit-receive steering vector;
- $\boldsymbol{b}(\theta_t) = \left[1, e^{j2\pi\frac{d}{\lambda_0}\sin(\theta_t)},\ldots,e^{j2\pi\frac{d}{\lambda_0}(N-1)\sin(\theta_t)}\right]^{\mathrm{T}} \in \mathbb{C}^N$ the angle-dependent receive steering vector, with $\lambda_0 = \frac{c}{f_0}$ the reference carrier wavelength;
- $\boldsymbol{c}(\theta_t) = \boldsymbol{R}^{\mathrm{T}}\boldsymbol{d}(\theta_t) \in \mathbb{C}^M$ the angle-dependent transmit steering vector;
- $\boldsymbol{R} \in \mathbb{C}^{M\times M}$ is the transmit waveforms correlation matrix, i.e., $R_{m,l} = \int_0^{T_p} x_m(s)\, x_l^*(s) ds$, $(m,l) \in \{1,...,M\}^2$;
- $\boldsymbol{d}(\theta_t) = \left[1, e^{j2\pi\frac{d}{\lambda_0}\sin(\theta_t)},\ldots,e^{j2\pi\frac{d}{\lambda_0}(M-1)\sin(\theta_t)}\right]^{\mathrm{T}} \in \mathbb{C}^M$ the angle-dependent transmit steering vector;
- $\boldsymbol{a}(\Delta\tau) = \left[1, e^{j2\pi\Delta f\Delta\tau}\ldots,e^{j2\pi\Delta f(M-1)\Delta\tau}\right]^{\mathrm{T}} \in \mathbb{C}^M$ the range-dependent steering vector.

Furthermore, letting $u = \sin(\theta_t)$ and $\delta = 2\Delta f\Delta\tau$ (satisfying $|\delta| \leq \frac{\Delta f}{B}$), $\boldsymbol{s}(\theta_t,\Delta\tau)$ can be further expressed as [23, 32]

$$\begin{aligned}\boldsymbol{s}(\theta_t,\Delta\tau) &= \boldsymbol{s}(u,\delta)\\ &= \boldsymbol{b}(u)\otimes[\boldsymbol{c}(u)\odot\boldsymbol{a}(\delta)],\end{aligned} \tag{5}$$

where

- $\boldsymbol{b}(u) = \left[1, e^{j2\pi\frac{d}{\lambda_0}u},\ldots,e^{j2\pi\frac{d}{\lambda_0}(N-1)u}\right]^{\mathrm{T}} \in \mathbb{C}^N$;

[1]For co-polarized channels r = t, and for cross-polarized channels r ≠ t. For a reciprocal medium (e.g., no Faraday rotation of polarization), $\Sigma_{\mathrm{VH}} = \Sigma_{\mathrm{HV}}$ [37].

[2]It is worth mentioning that FDA-MIMO radars generalize MIMO, and hence Frequency Division Multiplexing (FDM)-MIMO, architectures, since any MIMO signalling can be framed as FDA-MIMO waveform with a zero frequency-offset, i.e., $\Delta f = 0$. That said, to the best of Authors' knowledge, the main advantage of the FDA-MIMO is represented by its capability to embed in a simple way information on the actual target location into the data observed at the never ideal sampling time. Indeed, FDA-MIMO directly accounts for the unavoidable sampling time mismatches via the phase offsets on the different carriers imprinted on the probing waveforms. Such an exploitation is potentially feasible with an arbitrary set of MIMO waveforms, but would demand a deep comparison between the samples extracted on the different channels and the correlation matrix function of the actual transmitted signals, which is generally quite difficult to realize from a practical prospective.

[3]Note that the vector $\boldsymbol{\alpha}$ can be also expressed in terms of the polarization auxiliary angle and phase difference [4, 38].

- $\boldsymbol{c}(u) = \boldsymbol{R}^{\mathrm{T}}\boldsymbol{d}(u) \in \mathbb{C}^M$;
- $\boldsymbol{d}(u) = \left[1, e^{j2\pi\frac{d}{\lambda_0}u}, \ldots, e^{j2\pi\frac{d}{\lambda_0}(M-1)u}\right]^{\mathrm{T}} \in \mathbb{C}^M$;
- $\boldsymbol{a}(\delta) = \left[1, e^{j\pi\delta} \ldots, e^{j\pi(M-1)\delta}\right]^{\mathrm{T}} \in \mathbb{C}^M$.

Hence, defining the steering matrix $\boldsymbol{H}(u,\delta) = \begin{bmatrix} \mathbf{s}(u,\delta) & \mathbf{0} \\ \mathbf{0} & \mathbf{s}(u,\delta) \end{bmatrix} \in \mathbb{C}^{2MN\times 2}$, the useful polarimetric target echo (4) can be recast as

$$\boldsymbol{y}_{\mathrm{S}}(u,\delta) = \boldsymbol{\alpha} \otimes \boldsymbol{s}(u,\delta) = \boldsymbol{H}(u,\delta)\boldsymbol{\alpha}. \tag{6}$$

III. Formulation of the Detection Problem for Polarimetric FDA-MIMO Radar

This section investigates the problem of detecting a prospective target using a radar system equipped with a polarimetric FDA-MIMO. Let us define the received observation vector from the CUT (under the target presence) as $\boldsymbol{r} \in \mathbb{C}^{2MN}$, which contains the superposition of the polarimetric echo signal (6) of a prospective target and the interference plus noise contribution [39, 40]. Therefore, it can be cast as

$$\boldsymbol{r} = \boldsymbol{H}(u,\delta)\boldsymbol{\alpha} + \boldsymbol{m}, \tag{7}$$

where u, δ, and $\boldsymbol{\alpha}$ are regarded as unknown parameters and $\boldsymbol{m} \in \mathbb{C}^{2MN}$ is modeled as a zero-mean complex circularly symmetric Gaussian random vector, i.e., $\boldsymbol{m} \sim \mathcal{CN}(0, \boldsymbol{M})$, with $\boldsymbol{M} \in \mathbb{H}^{2MN}$ the positive definite polarimetric covariance matrix of the interference plus noise term. Let us also assume that a set of $K \geq 2MN$ secondary data $\boldsymbol{r}_k \in \mathbb{C}^{2MN}$, $k = 1, 2, \ldots, K$, free of useful target returns and with the same spectral characteristics as the interference from the CUT (homogeneous environment)[4], i.e., $\mathbb{E}[\boldsymbol{r}_k\boldsymbol{r}_k^{\dagger}] = \boldsymbol{M}$, $k = 1, 2, \ldots, K$, is available. As a consequence, the target detection problem can be formulated as a binary hypothesis test where the null hypothesis H_0 indicates the situation of target absence and H_1 represents the alternative, i.e.,

$$\begin{aligned} H_0 &: \begin{cases} \boldsymbol{r} = \boldsymbol{m} \\ \boldsymbol{r}_k = \boldsymbol{m}_k, \quad k = 1, 2, \ldots, K \end{cases} \\ H_1 &: \begin{cases} \boldsymbol{r} = \boldsymbol{H}(u,\delta)\boldsymbol{\alpha} + \boldsymbol{m} \\ \boldsymbol{r}_k = \boldsymbol{m}_k, \quad k = 1, 2, \ldots, K \end{cases} \end{aligned}. \tag{8}$$

Notably, the joint probability density functions (PDFs) of the observations under H_0 and H_1 are respectively given by

$$\begin{aligned} &f(\boldsymbol{r}, \boldsymbol{r}_1, \ldots, \boldsymbol{r}_K | \boldsymbol{M}; H_0) \\ &= \left\{ \frac{1}{\pi^{2MN}\det(\boldsymbol{M})} e^{-\mathrm{tr}\left(\boldsymbol{M}^{-1}\boldsymbol{R}_0\right)} \right\}^{K+1} \end{aligned} \tag{9a}$$

and

$$\begin{aligned} &f(\boldsymbol{r}, \boldsymbol{r}_1, \ldots, \boldsymbol{r}_K | \boldsymbol{\alpha}, u, \delta, \boldsymbol{M}; H_1) \\ &= \left\{ \frac{1}{\pi^{2MN}\det(\boldsymbol{M})} e^{-\mathrm{tr}\left(\boldsymbol{M}^{-1}\boldsymbol{R}_1\right)} \right\}^{K+1}, \end{aligned} \tag{9b}$$

[4]It worth mentioning that often a data selection stage of the $\boldsymbol{r}_k$ is also foreseen. This preprocessing is aimed at censoring from the training set data vectors containing possible outliers (sources of deviations from homogeneous assumption). The interested reader can refer to [41–43].

with $\boldsymbol{R}_0$ and $\boldsymbol{R}_1$ defined as

$$\boldsymbol{R}_0 = \frac{\boldsymbol{r}\boldsymbol{r}^{\dagger} + \sum_{k=1}^{K} \boldsymbol{r}_k\boldsymbol{r}_k^{\dagger}}{K+1} \tag{10a}$$

and

$$\boldsymbol{R}_1 = \frac{(\boldsymbol{r} - \boldsymbol{H}(u,\delta)\boldsymbol{\alpha})(\boldsymbol{r} - \boldsymbol{H}(u,\delta)\boldsymbol{\alpha})^{\dagger} + \sum_{k=1}^{K} \boldsymbol{r}_k\boldsymbol{r}_k^{\dagger}}{K+1}. \tag{10b}$$

Invoking the Neyman-Pearson framework [44], the optimal solution to the hypothesis testing problem (8), i.e., the Likelihood Ratio Test (LRT), cannot be implemented due to the unknowns $\boldsymbol{\alpha}$, u, δ, and $\boldsymbol{M}$. In this respect, some suboptimal and practically implementable architectures, based on the subspace GLRT [45] and 2SGLRT [46] frameworks, are proposed in subsection III-A and III-B, respectively.

A. Detection with GLRT

In this subsection, the design of a detector based on subspace GLRT framework [47] is investigated. In particular, the GLRT over the unknowns computes the decision statistic

$$\Lambda_{\mathrm{GLRT}} = \frac{\max\limits_{\boldsymbol{\alpha}, u\in\mathcal{A}, \delta\in\mathcal{B}, \boldsymbol{M}} f(\boldsymbol{r}, \boldsymbol{r}_1, \ldots, \boldsymbol{r}_K | \boldsymbol{\alpha}, u, \delta, \boldsymbol{M}; H_1)}{\max\limits_{\boldsymbol{M}} f(\boldsymbol{r}, \boldsymbol{r}_1, \cdots, \boldsymbol{r}_K | \boldsymbol{M}; H_0)}, \tag{11}$$

where, according to [23], $\mathcal{A}$ denotes the uncertainty set associated with u, i.e., $[-1, 1]$, and $\mathcal{B}$ that on δ, i.e., $\left[-\frac{\Delta f}{B}, \frac{\Delta f}{B}\right]$.

Maximizing both the numerator and the denominator of (11) over $\boldsymbol{M}$ yields (according to standard argumentation) [45]

$$\tau_{\mathrm{GLRT}} = \frac{1 + \boldsymbol{r}^{\dagger}\boldsymbol{S}^{-1}\boldsymbol{r}}{1 + \min\limits_{\boldsymbol{\alpha}, u\in\mathcal{A}, \delta\in\mathcal{B}} (\boldsymbol{r} - \boldsymbol{H}(u,\delta)\boldsymbol{\alpha})^{\dagger}\boldsymbol{S}^{-1}(\boldsymbol{r} - \boldsymbol{H}(u,\delta)\boldsymbol{\alpha})} \underset{H_0}{\overset{H_1}{\gtrless}} \xi, \tag{12}$$

where $\mathbf{S} = \sum_{k=1}^{K} \boldsymbol{r}_k\boldsymbol{r}_k^{\dagger} \in \mathbb{C}^{2MN\times 2MN}$ and ξ denotes the detection threshold, set to ensure the desired probability of false alarm (P_{fa}). Letting for notation simplicity $\boldsymbol{H}(u,\delta) = \boldsymbol{H}$, replacing $\boldsymbol{\alpha}$ with its ML estimate yields

$$\frac{1 + \boldsymbol{r}^{\dagger}\boldsymbol{S}^{-1}\boldsymbol{r}}{1 + \boldsymbol{r}^{\dagger}\boldsymbol{S}^{-1}\boldsymbol{r} - \max\limits_{u\in\mathcal{A}, \delta\in\mathcal{B}} g(u,\delta)} \underset{H_0}{\overset{H_1}{\gtrless}} \xi, \tag{13}$$

where[5]

$$g(u,\delta) = \boldsymbol{r}^{\dagger}\boldsymbol{S}^{-1}\boldsymbol{H}\left[\boldsymbol{H}^{\dagger}\boldsymbol{S}^{-1}\boldsymbol{H}\right]^{-1}\boldsymbol{H}^{\dagger}\boldsymbol{S}^{-1}\boldsymbol{r}. \tag{14}$$

Evidently, (13) is statistically equivalent to

$$\tau_{\mathrm{GLRT}} = \frac{1}{1 + \boldsymbol{r}^{\dagger}\boldsymbol{S}^{-1}\boldsymbol{r}} \max_{u\in\mathcal{A}, \delta\in\mathcal{B}} g(u,\delta) \underset{H_0}{\overset{H_1}{\gtrless}} \xi. \tag{15}$$

B. Detection with 2SGLRT

In this subsection, using the conventional approach of assuming the interference covariance matrix known at the

[5]With some abuse of notation, the same ξ is used to denote the different detection thresholds for both the GLRT and the 2step-GLRT decision statistics (12), (13), (15), (19), (20), (22), and (23).

design stage, an Adaptive Matched Filter (AMF)-like detector (also known as the 2SGLRT) is derived. Precisely, the GLRT decision statistic for known covariance matrix is given by [46]

$$\Lambda = \frac{\max\limits_{\boldsymbol{\alpha},u\in\mathcal{A},\delta\in\mathcal{B}} \bar{f}(\boldsymbol{r}|\boldsymbol{\alpha},u,\delta,\boldsymbol{M};H_1)}{\bar{f}(\boldsymbol{r}|\boldsymbol{M};H_0)}, \tag{16}$$

where

$$\bar{f}(\boldsymbol{r}|\boldsymbol{M};H_0) = \frac{1}{\pi^{2MN}\det(\boldsymbol{M})} e^{-\boldsymbol{r}^\dagger \boldsymbol{M}^{-1}\boldsymbol{r}} \tag{17a}$$

and

$$\begin{aligned}&\bar{f}(\boldsymbol{r}|\boldsymbol{\alpha},u,\delta,\boldsymbol{M};H_1)\\ &= \frac{1}{\pi^{2MN}\det(\boldsymbol{M})} e^{-(\boldsymbol{r}-\boldsymbol{H}(u,\delta)\boldsymbol{\alpha})^\dagger \boldsymbol{M}^{-1}(\boldsymbol{r}-\boldsymbol{H}(u,\delta)\boldsymbol{\alpha})}.\end{aligned} \tag{17b}$$

Hence, substituting the ML estimate of the unknown $\boldsymbol{\alpha}$, i.e.,

$$\hat{\boldsymbol{\alpha}} = \left[\boldsymbol{H}^\dagger \boldsymbol{M}^{-1}\boldsymbol{H}\right]^{-1} \boldsymbol{H}^\dagger \boldsymbol{M}^{-1}\boldsymbol{r}. \tag{18}$$

into (16), the following decision rule is obtained

$$\begin{aligned}&\tau_{\text{2SGLRT}} =\\ &\max_{u\in\mathcal{A},\delta\in\mathcal{B}} \boldsymbol{r}^\dagger \boldsymbol{M}^{-1}\boldsymbol{H}\left[\boldsymbol{H}^\dagger \boldsymbol{M}^{-1}\boldsymbol{H}\right]^{-1} \boldsymbol{H}^\dagger \boldsymbol{M}^{-1}\boldsymbol{r} \underset{H_0}{\overset{H_1}{\gtrless}} \xi.\end{aligned} \tag{19}$$

Finally, using the sample covariance matrix $\hat{\boldsymbol{M}} = \frac{1}{K}\boldsymbol{S}$ in lieu of $\boldsymbol{M}$ yields

$$\tau_{\text{2SGLRT}} = \max_{u\in\mathcal{A},\delta\in\mathcal{B}} g(u,\delta) \underset{H_0}{\overset{H_1}{\gtrless}} \xi. \tag{20}$$

IV. Optimization Problem (20)

This section is devoted to the development of some optimization strategies to handle

$$\max_{u\in\mathcal{A},\delta\in\mathcal{B}} g(u,\delta), \tag{21}$$

namely, to compute the ML estimate of the target location parameters under the H_1 hypothesis. To this end, let us preliminary observe that (21) falls in the class of box-constrained optimization problems. Moreover, an approximated solution based on a 2-D grid search is characterized by a high and often impractical computational cost if the grid size is sufficiently dense to get a close to optimum objective value. This motivates the design of some optimization methods pursuing reduced-complexity sub-optimal solutions. In this regard, three strategies are developed:

1) the LAM procedure [33];
2) the GPM [34];
3) the CD Method [35].

Denoting by $(\hat{u},\hat{\delta})$ the estimate of the unknowns using one of the aforementioned LAM, GPM, and CD methods, it follows that the actual decision rules, based on the GLRT and 2SGLRT criteria, are given by

$$\tau_{\text{GLRT}} = \frac{1}{1+\boldsymbol{r}^\dagger \boldsymbol{S}^{-1}\boldsymbol{r}} g(\hat{u},\hat{\delta}) \underset{H_0}{\overset{H_1}{\gtrless}} \xi \tag{22}$$

and

$$\tau_{\text{2SGLRT}} = g(\hat{u},\hat{\delta}) \underset{H_0}{\overset{H_1}{\gtrless}} \xi, \tag{23}$$

respectively.

A. Linearized Array Manifold (LAM) Method

Resorting to the array manifold linearization approach proposed in [33], a sub-optimal and approximated solution method to the optimization problem in (21) is derived. To this end, let us observe that (21) is equivalent to

$$\min_{\boldsymbol{\alpha},u\in\mathcal{A},\delta\in\mathcal{B}} (\boldsymbol{r}-\boldsymbol{H}(u,\delta)\boldsymbol{\alpha})^\dagger \boldsymbol{S}^{-1}(\boldsymbol{r}-\boldsymbol{H}(u,\delta)\boldsymbol{\alpha}), \tag{24}$$

namely, given a maximizer $u_1^\star, \delta_1^\star$ of (21), an optimal solution to (24) is given by

$$\boldsymbol{\alpha}_2^\star = \left[\boldsymbol{H}(u_1^\star,\delta_1^\star)^\dagger \boldsymbol{S}^{-1}\boldsymbol{H}(u_1^\star,\delta_1^\star)\right]^{-1} \boldsymbol{H}(u_1^\star,\delta_1^\star)^\dagger \boldsymbol{S}^{-1}\boldsymbol{r}, \tag{25a}$$

$$u_2^\star = u_1^\star, \tag{25b}$$

$$\delta_2^\star = \delta_1^\star. \tag{25c}$$

In a similar manner, given the minimizer $\boldsymbol{\alpha}_2^\star, u_2^\star, \delta_2^\star$ of (24), an optimal solution to (21) is $u_1^\star = u_2^\star$ and $\delta_1^\star = \delta_2^\star$.

Now, given the nominal angle and incremental range $\bar{u}$ and $\bar{\delta}$, the actual mismatch w.r.t. the true target parameters values can be accounted by performing a tailored linearization of the array steering matrix $\boldsymbol{H}(u,\delta)$ around $\bar{u}$ and $\bar{\delta}$. To this end, denoting by $(\Delta u, \Delta\delta)$ the angle and range offsets, i.e., $\Delta u = u - \bar{u}$, $\Delta\delta = \delta - \bar{\delta}$, the array steering matrix can be approximated at the first order as

$$\begin{aligned}&\boldsymbol{H}_a(\Delta\boldsymbol{\theta}) = \boldsymbol{H}_a(\Delta u,\Delta\delta)\\ &\simeq \boldsymbol{H}(\bar{u},\bar{\delta}) + \left.\frac{\partial \boldsymbol{H}(u,\delta)}{\partial u}\right|_{(\bar{u},\bar{\delta})} \Delta u + \left.\frac{\partial \boldsymbol{H}(u,\delta)}{\partial \delta}\right|_{(\bar{u},\bar{\delta})} \Delta\delta\\ &= \bar{\boldsymbol{H}} + \bar{\boldsymbol{H}}_u \Delta u + \bar{\boldsymbol{H}}_\delta \Delta\delta,\end{aligned} \tag{26}$$

with $\Delta\boldsymbol{\theta} = [\Delta u, \Delta\delta]^{\mathrm{T}} \in \mathbb{R}^2$. Detailed expressions for $\boldsymbol{H}_u = \frac{\partial \boldsymbol{H}(u,\delta)}{\partial u}$ and $\boldsymbol{H}_\delta = \frac{\partial \boldsymbol{H}(u,\delta)}{\partial \delta}$ are reported in Appendix A. Hence, resorting to the linearization procedure, an optimized solution to (24) can be obtained solving

$$\min_{\boldsymbol{\alpha},\Delta\boldsymbol{\theta}\in\mathcal{C}} (\boldsymbol{r}-\boldsymbol{H}_a(\Delta\boldsymbol{\theta})\boldsymbol{\alpha})^\dagger \boldsymbol{S}^{-1}(\boldsymbol{r}-\boldsymbol{H}_a(\Delta\boldsymbol{\theta})\boldsymbol{\alpha}), \tag{27}$$

where $\mathcal{C} = [-\kappa,\kappa]\times[-\rho,\rho]$, with $\kappa = 1$ and $\rho = \frac{\Delta f}{B}$, is the nonempty and compact feasible set[6]. In this respect, a CD-based procedure is proposed to solve the optimization problem (27) by alternatively optimizing $\boldsymbol{\alpha}$ and $\Delta\boldsymbol{\theta}$ up to convergence. In the following, the analytical solutions to the resulting optimization problems, at the h-th iteration, are derived.

a) Optimization w.r.t. $\boldsymbol{\alpha}$.
At the h-th iteration, the optimization problem w.r.t. $\boldsymbol{\alpha}$ is given by

$$\begin{aligned}\min_{\boldsymbol{\alpha}}\ &(\boldsymbol{r}-\boldsymbol{H}_a(\Delta\boldsymbol{\theta}^{(h-1)})\boldsymbol{\alpha})^\dagger \boldsymbol{S}^{-1}\\ &(\boldsymbol{r}-\boldsymbol{H}_a(\Delta\boldsymbol{\theta}^{(h-1)})\boldsymbol{\alpha}),\end{aligned} \tag{28}$$

[6]Note that the accuracy of the approximation can be improved considering a partition of the original feasible set $\mathcal{C}$ into D subsets, $\mathcal{C}_i, i = 1,\ldots,D$, and performing the linearization of the steering matrix around different nominal points $(\bar{u}_i,\bar{\delta}_i), i = 1,\ldots,D$, each associated to a specific uncertainty set $\mathcal{C}_i, i = 1,\ldots,D$.

whose optimal solution is

$$\boldsymbol{\alpha}^{(h)} = \left(\boldsymbol{H}_a^{\dagger}\left(\Delta\boldsymbol{\theta}^{(h-1)}\right)\boldsymbol{S}^{-1}\boldsymbol{H}_a\left(\Delta\boldsymbol{\theta}^{(h-1)}\right)\right)^{-1} \boldsymbol{H}_a^{\dagger}\left(\Delta\boldsymbol{\theta}^{(h-1)}\right)\boldsymbol{S}^{-1}\boldsymbol{r}. \tag{29}$$

b) Optimization w.r.t. $\Delta\boldsymbol{\theta}$.
At the h-th iteration, the optimization w.r.t. $\Delta\boldsymbol{\theta}$ yields

$$\begin{aligned}&\min_{\substack{|\Delta u|\le\kappa\\|\Delta\delta|\le\rho}} (\boldsymbol{r}-(\bar{\boldsymbol{H}}+\bar{\boldsymbol{H}}_u\Delta u+\bar{\boldsymbol{H}}_\delta\Delta\delta)\boldsymbol{\alpha}^{(h)})^{\dagger}\boldsymbol{S}^{-1} \\ &\qquad (\boldsymbol{r}-(\bar{\boldsymbol{H}}+\bar{\boldsymbol{H}}_u\Delta u+\bar{\boldsymbol{H}}_\delta\Delta\delta)\boldsymbol{\alpha}^{(h)}) \\ &= \min_{\Delta\boldsymbol{\theta}\in\mathcal{C}} (\tilde{\boldsymbol{r}}-\tilde{\boldsymbol{H}}\Delta\boldsymbol{\theta})^{\dagger}\boldsymbol{S}^{-1}(\tilde{\boldsymbol{r}}-\tilde{\boldsymbol{H}}\Delta\boldsymbol{\theta}) \\ &= \min_{\Delta\boldsymbol{\theta}\in\mathcal{C}} (\hat{\boldsymbol{r}}-\hat{\boldsymbol{H}}\Delta\boldsymbol{\theta})^{\dagger}(\hat{\boldsymbol{r}}-\hat{\boldsymbol{H}}\Delta\boldsymbol{\theta}),\end{aligned} \tag{30}$$

where

- $\tilde{\boldsymbol{r}} = \boldsymbol{r} - \bar{\boldsymbol{H}}\boldsymbol{\alpha}^{(h)}$;
- $\tilde{\boldsymbol{H}} = \left[\bar{\boldsymbol{H}}_u\boldsymbol{\alpha}^{(h)}, \bar{\boldsymbol{H}}_\delta\boldsymbol{\alpha}^{(h)}\right]$;
- $\hat{\boldsymbol{r}} = \boldsymbol{S}^{-1/2}\tilde{\boldsymbol{r}}$;
- $\hat{\boldsymbol{H}} = [\hat{\boldsymbol{h}}_u, \hat{\boldsymbol{h}}_\delta] = \boldsymbol{S}^{-1/2}\tilde{\boldsymbol{H}}$.

The following proposition provides an optimal point to (30).

***Proposition** 1: An optimal solution $\Delta\boldsymbol{\theta}^{(h)}$ to* (30) *is*

$$\Delta\boldsymbol{\theta}_1 = \left[\Re\{\hat{\boldsymbol{H}}^{\dagger}\hat{\boldsymbol{H}}\}\right]^{-1}\Re\{\hat{\boldsymbol{H}}^{\dagger}\hat{\boldsymbol{r}}\} \tag{31}$$

if it is feasible. Otherwise, it can be computed as

$$\Delta\boldsymbol{\theta}^{(h)} = \underset{\Delta\boldsymbol{\theta}\in\{\Delta\boldsymbol{\theta}_i\}_{i=2}^{5}}{\arg\min}\ (\hat{\boldsymbol{r}}-\hat{\boldsymbol{H}}\Delta\boldsymbol{\theta})^{\dagger}(\hat{\boldsymbol{r}}-\hat{\boldsymbol{H}}\Delta\boldsymbol{\theta}), \tag{32}$$

where $\Delta\boldsymbol{\theta}_i$, $i=2,\ldots,5$ are candidate solutions given by

$$\begin{aligned}\Delta\boldsymbol{\theta}_2 &= [\kappa, \Delta\delta_+^*]^{\mathrm{T}}, \quad \Delta\boldsymbol{\theta}_3 = [-\kappa, \Delta\delta_-^*]^{\mathrm{T}}, \\ \Delta\boldsymbol{\theta}_4 &= [\Delta u_+^*, \rho]^{\mathrm{T}}, \quad \Delta\boldsymbol{\theta}_5 = [\Delta u_-^*, -\rho]^{\mathrm{T}},\end{aligned} \tag{33}$$

with

$$\Delta u_{\pm}^* = \min\left(\kappa, \max\left(\frac{\Re\{(\hat{\boldsymbol{r}}^{\dagger} - \hat{\boldsymbol{h}}_{\delta}^{\dagger}(\pm\rho))\,\hat{\boldsymbol{h}}_u\}}{\|\hat{\boldsymbol{h}}_u\|^2}, -\kappa\right)\right) \tag{34}$$

and

$$\Delta\delta_{\pm}^* = \min\left(\rho, \max\left(\frac{\Re\{(\hat{\boldsymbol{r}}^{\dagger} - \hat{\boldsymbol{h}}_{u}^{\dagger}(\pm\kappa))\,\hat{\boldsymbol{h}}_\delta\}}{\|\hat{\boldsymbol{h}}_\delta\|^2}, -\rho\right)\right). \tag{35}$$

Proof: See Appendix B. ∎

A summary of the devised procedure to determine a solution to (27) is reported in **Algorithm 1**, where the exit condition is set as $|P^{(h)} - P^{(h-1)}| < \varepsilon_1$, with $\varepsilon_1 > 0$ and

$$\begin{aligned}P^{(h)} =&(\boldsymbol{r}-\boldsymbol{H}_a(\Delta\boldsymbol{\theta}^{(h)})\boldsymbol{\alpha}^{(h)})^{\dagger}\boldsymbol{S}^{-1} \\ &(\boldsymbol{r}-\boldsymbol{H}_a(\Delta\boldsymbol{\theta}^{(h)})\boldsymbol{\alpha}^{(h)}).\end{aligned} \tag{36}$$

Now, given the output of **Algorithm 1**, an estimate of the target angle and incremental range can be obtained as $\tilde{u}_{\mathrm{LAM}} = \bar{u} + \Delta u^{\star}$ and $\tilde{\delta}_{\mathrm{LAM}} = \bar{\delta} + \Delta\delta^{\star}$, respectively, with $\Delta u^{\star}$ and $\Delta\delta^{\star}$ the resulting mismatch estimates w.r.t. the nominal values $\bar{u}$ and $\bar{\delta}$, respectively. However, $[\tilde{u}_{\mathrm{LAM}}, \tilde{\delta}_{\mathrm{LAM}}]^{\mathrm{T}}$ could not be a feasible solution to (21). To this end, the final estimate of the target location parameters undergoes a projection in the feasible set by $\hat{\boldsymbol{h}}_{\mathrm{LAM}} = \left[\hat{u}_{\mathrm{LAM}}, \hat{\delta}_{\mathrm{LAM}}\right]^{\mathrm{T}} = \boldsymbol{P}_{\mathcal{C}}\left([\tilde{u}_{\mathrm{LAM}}, \tilde{\delta}_{\mathrm{LAM}}]^{\mathrm{T}}\right)$, where $\boldsymbol{P}_{\mathcal{C}}$ is the projection operator onto the constraint set $\mathcal{C}$,

Algorithm 1 FDA-LAM

Input: $\boldsymbol{r}, \boldsymbol{S}, \bar{u}, \bar{\delta}, \kappa, \rho, \varepsilon_1$.
Output: $\hat{\boldsymbol{h}}_{\mathrm{LAM}}$.

1. Set $h=0$, $\Delta\boldsymbol{\theta}^{(h)} = [\Delta u^{(h)}, \Delta\delta^{(h)}]^{\mathrm{T}} = \boldsymbol{0}$, $P^{(h)} = \infty$.
2. **repeat**
3. $h = h+1$;
4. Compute $\boldsymbol{\alpha}^{(h)}$ via (29);
5. Compute $\Delta\boldsymbol{\theta}^{(h)}$ via Proposition 1;
6. Evaluate $P^{(h)} = (\boldsymbol{r}-\boldsymbol{H}_a(\Delta\boldsymbol{\theta}^{(h)})\boldsymbol{\alpha}^{(h)})^{\dagger}\boldsymbol{S}^{-1}(\boldsymbol{r}-\boldsymbol{H}_a(\Delta\boldsymbol{\theta}^{(h)})\boldsymbol{\alpha}^{(h)})$
7. **until** $|P^{(h)} - P^{(h-1)}| < \varepsilon_1$.
8. $\Delta\boldsymbol{\theta}^{\star} = [\Delta u^{\star}, \Delta\delta^{\star}]^{\mathrm{T}} = \Delta\boldsymbol{\theta}^{(h)}$
9. Output $\hat{\boldsymbol{h}}_{\mathrm{LAM}} = \boldsymbol{P}_{\mathcal{C}}\left([\bar{u}+\Delta u^{\star}, \bar{\delta}+\Delta\delta^{\star}]^{\mathrm{T}}\right)$.

i.e.,

$$\boldsymbol{P}_{\mathcal{C}}\left([\tilde{u},\tilde{\delta}]^{\mathrm{T}}\right) = \begin{bmatrix}\min\{\max\{\tilde{u}, -\kappa\}, \kappa\} \\ \min\left\{\max\left\{\tilde{\delta}, -\rho\right\}, \rho\right\}\end{bmatrix}, \tilde{u}, \tilde{\delta} \in \mathbb{R}. \tag{37}$$

B. Gradient Projection Method (GPM)

A procedure to tackle the maximization problem (21) is devised resorting to an ascent direction method. Specifically, an estimate of $\boldsymbol{h}$ could be computed iteratively via the projected gradient technique [34]. Accordingly, at the k-th iteration, an updated estimate is obtained moving from the previously estimated point $\boldsymbol{h}_{k-1}$ along the current ascent direction (given by the gradient evaluated at $\boldsymbol{h}_{k-1}$) and then projecting the resulting point onto the considered convex set $\mathcal{C}$. Precisely,

$$\boldsymbol{h}_k = \boldsymbol{P}_{\mathcal{C}}\left(\boldsymbol{h}_{k-1} + \eta_k\boldsymbol{g}_{\triangle}(\boldsymbol{h}_{k-1})\right), \tag{38}$$

where

- $\boldsymbol{h}_0 \in \mathbb{R}^2$ is the initial vector;
- $\boldsymbol{h}_{k-1} = [u_{k-1}, \delta_{k-1}]^{\mathrm{T}} \in \mathbb{R}^2$ with u_{k-1} and δ_{k-1} the estimates at the $(k-1)$-th iteration;
- η_k the step size;
- $\boldsymbol{g}_{\triangle}(\boldsymbol{h}_{k-1}) = \left[\frac{\partial g(u,\delta)}{\partial u}, \frac{\partial g(u,\delta)}{\partial\delta}\right]^{\mathrm{T}}\Big|_{(u_{k-1},\delta_{k-1})}$ the gradient of $g(u,\delta)$ evaluated at u_{k-1} and δ_{k-1} (see Appendix C for its computation);
- $\boldsymbol{P}_{\mathcal{C}}$ is defined as in (37).

Note that η_k can be either a constant stepsize $\bar{\eta} \in (0, \frac{2}{L})$, with L the smallest Lipschitz constant for $g(\boldsymbol{h}) = g(u,\delta)$, or chosen adaptively by means of the backtracking procedure [34], i.e.,

$$\begin{cases}\eta_k^{\mathrm{cons}} = \bar{\eta}, & \text{constant stepsize} \\ \eta_k^{\mathrm{back}} = s\beta^{i_k}, & \text{backtracking}\end{cases}, \tag{39}$$

where i_k the smallest nonnegative integer satisfying

$$g(\tilde{\boldsymbol{h}}^{(i_k)}) - g(\boldsymbol{h}_{k-1}) \ge \zeta s\beta^{i_k}\left\|\boldsymbol{G}_{\frac{1}{s\beta^{i_k}}}(\boldsymbol{h}_{k-1})\right\|^2, \tag{40}$$

with $s > 0$, $\zeta \in (0,1)$, and $\beta \in (0,1)$ algorithm tuning parameters,

$$\tilde{\boldsymbol{h}}^{(i_k)} = \boldsymbol{P}_{\mathcal{C}}\left(\boldsymbol{h}_{k-1} + s\beta^{i_k}\boldsymbol{g}_{\triangle}(\boldsymbol{h}_{k-1})\right) \tag{41}$$

Algorithm 2 FDA-GPM

Input: $\boldsymbol{r}, \boldsymbol{S}, \bar{u}, \bar{\delta}, s, \beta, \zeta, \varepsilon_2$.
Output: $\hat{\boldsymbol{h}}_{\rm GPM}$.

1. Set $k=0$, $\boldsymbol{h}_k = \boldsymbol{h}_0 = [\bar{u}, \bar{\delta}]^{\rm T}$.
2. **repeat**
3. $k = k+1$;
4. Update η_k using either a constant or adaptive (via backtracking strategy) stepsize (39);
5. Compute $\boldsymbol{h}_k$ via (38);
6. **until** $\|\boldsymbol{h}_k - \boldsymbol{h}_{k-1}\| < \varepsilon_2$.
7. Output $\hat{\boldsymbol{h}}_{\rm GPM} = \left[\hat{u}_{\rm GPM}, \hat{\delta}_{\rm GPM}\right]^{\rm T} = \boldsymbol{h}_k$.

and

$$\boldsymbol{G}_{\varkappa}(\boldsymbol{h}) = \varkappa \left[\boldsymbol{h} - \boldsymbol{P}_{\mathcal{C}}\left(\boldsymbol{h} + \frac{1}{\varkappa}\boldsymbol{g}_{\triangle}(\boldsymbol{h})\right)\right] \tag{42}$$

the gradient mapping with $\varkappa > 0$.

Algorithm 2 summarizes the gradient projection procedure, where the exit condition is set as $\|\boldsymbol{h}_k - \boldsymbol{h}_{k-1}\| < \varepsilon_2$, with $\varepsilon_2 > 0$. Besides, the resulting estimate is denoted by $\hat{\boldsymbol{h}}_{\rm GPM} = \left[\hat{u}_{\rm GPM}, \hat{\delta}_{\rm GPM}\right]^{\rm T}$.

Remark 1. Before concluding this subsection, the convergence of the GPM is examined via the following lemma [34, Th. 9.14], reformulated for the case of a maximization problem.

Lemma 4.1: Consider the optimization problem

$$\mathcal{P}\begin{cases}\max & g(\boldsymbol{h}) \\ \text{s.t.} & \boldsymbol{h} \in \mathcal{C}\end{cases}, \tag{43}$$

where $g(\boldsymbol{h}) \in C_L^{1,1}$ is bounded above and $\mathcal{C}$ is a closed and convex set. Let $\{\boldsymbol{h}_k\}_{k\geq 0}$ be the sequence generated by the GPM w.r.t. problem $\mathcal{P}$ using either constant or adaptive (backtracking) stepsize. Then

- the sequence $\{g(\boldsymbol{h}_k)\}_{k\geq 0}$ is nondecreasing and $g(\boldsymbol{h}_k) > g(\boldsymbol{h}_{k-1})$ unless $\boldsymbol{h}_{k-1}$ is a stationary point of $\mathcal{P}$;
- any limit point $\boldsymbol{h}^\star$ of $\{\boldsymbol{h}_k\}_{k\geq 0}$ is a stationary point of $\mathcal{P}$.

■

Exploiting the above result, the convergence of **Algorithm 2** to a stationary point of problem (21) is guaranteed, provided that $g(u,\delta) \in C_L^{1,1}$ (see Appendix D for the detailed proof).

C. Coordinate Descent (CD) Method

The CD method [35, 48] is an iterative procedure that exploits a series of 1-D searches, with one variable optimized at a time while keeping the other constant. Precisely, the searches w.r.t. u and δ are respectively conducted over $\mathcal{I}_u$ and $\mathcal{I}_\delta$ (corresponding to the discretized versions of $\mathcal{A}$ and $\mathcal{B}$ with (N_u+1) and $(N_\delta+1)$ points, respectively), defined as [23]

$$\mathcal{I}_u = \left\{-1 + \frac{2i}{N_u},\ i = 0, \ldots, N_u\right\} \tag{44a}$$

and

$$\mathcal{I}_\delta = \left\{-\frac{\Delta f}{B} + \frac{2i}{N_\delta}\frac{\Delta f}{B},\ i = 0, \ldots, N_\delta\right\}. \tag{44b}$$

Algorithm 3 FDA-CD

Input: $\boldsymbol{r}$, $\boldsymbol{S}$, $\bar{u}$, $\bar{\delta}$, $\mathcal{I}_u$, $\mathcal{I}_\delta$, ε_3.
Output: $\hat{\boldsymbol{h}}_{\rm CD}$.

1. Set $k=0$, $\hat{u}^k = \bar{u}$, $\hat{\delta}^k = \bar{\delta}$, $g^k = g(\hat{u}^k, \hat{\delta}^k)$
2. **repeat** (optimization for initial search direction given by u)
3. Find $\hat{u}^{k+1} = \underset{u\in\mathcal{I}_u}{\arg\max}\, g(u, \hat{\delta}^k)$;
4. Find $\hat{\delta}^{k+1} = \underset{\delta\in\mathcal{I}_\delta}{\arg\max}\, g(\hat{u}^{k+1}, \delta)$ and set g^{k+1} as the corresponding maximum value;
5. $k = k+1$;
6. **until** $|g^k - g^{k-1}| < \varepsilon_3$;
7. $g_x = g^k$; $\hat{u}_x = \hat{u}^k$; $\hat{\delta}_x = \hat{\delta}^k$;
8. Set $k=0$;
9. **repeat** (optimization for initial search direction given by δ)
10. Find $\hat{\delta}^{k+1} = \underset{\delta\in\mathcal{I}_\delta}{\arg\max}\, g(\hat{u}^k, \delta)$;
11. Find $\hat{u}^{k+1} = \underset{u\in\mathcal{I}_u}{\arg\max}\, g(u, \hat{\delta}^{k+1})$ and set g^{k+1} as the corresponding maximum value;
12. $k = k+1$;
13. **until** $|g^k - g^{k-1}| < \varepsilon_3$;
14. $g_y = g^k$; $\hat{u}_y = \hat{u}^k$; $\hat{\delta}_y = \hat{\delta}^k$;
15. **if** $g_x > g_y$
16. Output $\hat{\boldsymbol{h}}_{\rm CD} = \left[\hat{u}_{\rm CD}, \hat{\delta}_{\rm CD}\right]^{\rm T} = [\hat{u}_x, \hat{\delta}_x]^{\rm T}$.
17. **else**
18. Output $\hat{\boldsymbol{h}}_{\rm CD} = \left[\hat{u}_{\rm CD}, \hat{\delta}_{\rm CD}\right]^{\rm T} = [\hat{u}_y, \hat{\delta}_y]^{\rm T}$.
19. **end**

Remarkably, since the order of the optimization could lead to different solutions, both the instances of optimizing first u and then over δ, and first δ and then over u, are implemented, with the optimal estimate chosen between the resulting two solutions.

Denoting by $g^k = g\left(\hat{u}^k, \hat{\delta}^k\right)$ and setting the nominal values as initial estimates, i.e., $\hat{u}^0 = \bar{u}$ and $\hat{\delta}^0 = \bar{\delta}$, u and δ can be updated according to **Algorithm 3**, where the exit condition is set as $|g^k - g^{k-1}| < \varepsilon_3$, with $\varepsilon_3 > 0$. Hence, the final solution using the CD method is obtained as $\hat{\boldsymbol{h}}_{\rm CD} = \left[\hat{u}_{\rm CD}, \hat{\delta}_{\rm CD}\right]^{\rm T}$.

Note that for any initial search direction, i.e., along the u or δ domain, the CD approach (starting from the second iteration) coincides with the Maximum Block Improvement (MBI) policy [49]. Therefore, invoking the convergence properties of MBI [49–51], any limit point resulting from **Algorithm 3** (assuming an exact optimization at each step) is a stationary point to Problem (21), although its convergence to the optimal value cannot be claimed [35].

D. Bounded CFARness Analysis of the Derived Detectors and Computational Complexities

In this subsection, the bounded CFAR property of the proposed detection architectures is studied. First of all, from (12) it is straightforward to see that the GLRT decision statistic is

This article has been accepted for publication in IEEE Transactions on Aerospace and Electronic Systems. This is the author's version which has not been fully edited and content may change prior to final publication. Citation information: DOI 10.1109/TAES.2022.3210887

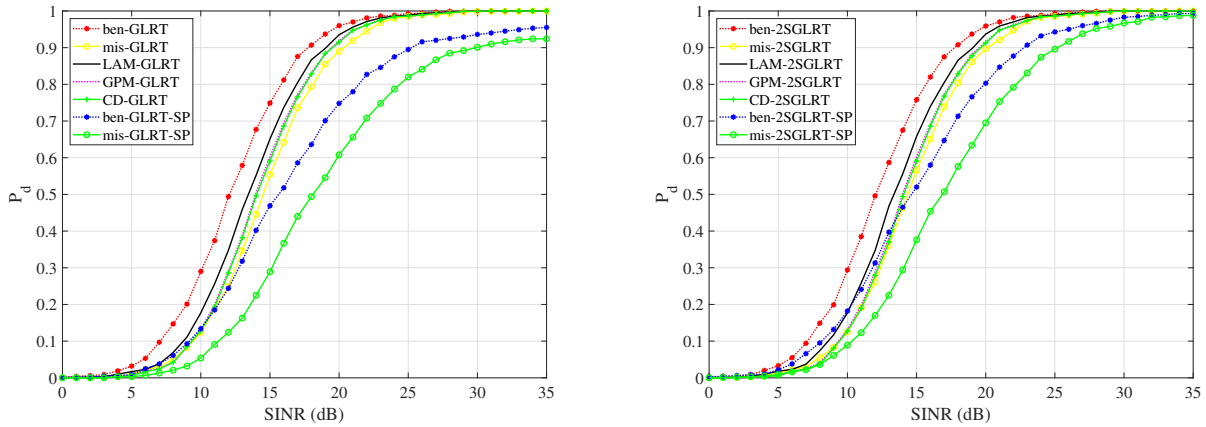

Fig. 3: Detection performance for white noise, assuming $K = 320$ and the parameters of Table I. Fig. (a) considers the GLRT-based detectors, whereas Fig. (b) reports the 2SGLRT-based counterparts.

upper bounded by a CFAR detector, i.e.,

$$\tau_{\mathrm{GLRT}} \leq 1 + \boldsymbol{r}^{\dagger}\boldsymbol{S}^{-1}\boldsymbol{r} = \tau_{\mathrm{CFAR}}. \tag{45}$$

Similarly, with reference to the 2SGLRT detector (20), the following inequality applies, i.e.,

$$1 + \tau_{\mathrm{2SGLRT}} \leq \tau_{\mathrm{CFAR}}. \tag{46}$$

As a consequence, the devised decision architectures ensure the bounded CFAR property, i.e.,

$$\begin{aligned} P_{fa,\mathrm{GLRT}} =& \Pr(\tau_{\mathrm{GLRT}} > \xi|\mathrm{H}_0) \\ &\leq \Pr(\tau_{\mathrm{CFAR}} > \xi|\mathrm{H}_0), \end{aligned} \tag{47}$$

and

$$\begin{aligned} P_{fa,\mathrm{2SGLRT}} =& \Pr(\tau_{\mathrm{2SGLRT}}+1 > \xi|\mathrm{H}_0) \\ &\leq \Pr(\tau_{\mathrm{CFAR}} > \xi|\mathrm{H}_0). \end{aligned} \tag{48}$$

Hence, for each considered decision strategies, it is always possible to set a universal threshold ξ (based on just the system parameters) for which $\Pr(\tau_{\mathrm{CFAR}} > \xi|\mathrm{H}_0)$ achieves a desired upper bound $\bar{P}_{fa}$ to the actual P_{fa}. Evidently, this property holds true also for an approximated implementation of the decision statistics in (12) and (20), when possible sub-optimal solution methods are employed to estimate the unknown target parameters $\boldsymbol{\alpha}$, u, and δ.

Finally, as long as the number of iterations involved in the three optimization procedures keeps quite limited, the computational complexity is dominated by the evaluation of the sample covariance matrix $\boldsymbol{S}$, which demands $\mathcal{O}\left(M^2N^2K\right)$ operations, regardless of the adopted optimization strategy.

V. Simulation Results

In this section, numerical examples are provided to evaluate the performance of the proposed target detection methods for the polarimetric FDA-MIMO radar. In the following, orthogonal baseband signals are assumed, i.e., $\boldsymbol{R} = \boldsymbol{I}$.

The P_d is used as figure of merit to assess the detection performance, which is estimated resorting to 1000 independent Monte Carlo (MC) runs assuming a $P_{fa} = 10^{-4}$. Besides, the detection thresholds are computed using $100/P_{fa}$ independent trials. The SINR is defined as

$$\mathrm{SINR} = \mathbb{E}[\boldsymbol{\alpha}^{\dagger}\boldsymbol{H}^{\dagger}\boldsymbol{M}^{-1}\boldsymbol{H}\boldsymbol{\alpha}] = \gamma^2\mathrm{tr}(\boldsymbol{\Sigma}_t\boldsymbol{H}^{\dagger}\boldsymbol{M}^{-1}\boldsymbol{H}), \tag{49}$$

where $\mathbb{E}[\boldsymbol{\alpha}\boldsymbol{\alpha}^{\dagger}] = \gamma^2\boldsymbol{\Sigma}_t$, with $\boldsymbol{\Sigma}_t = \begin{bmatrix} 1 & \epsilon_t\sqrt{\delta_t} \\ \epsilon_t^*\sqrt{\delta_t} & \delta_t \end{bmatrix} \in \mathbb{C}^{2\times 2}$ and γ rules the target strength, respectively. Besides, in the reported results it is assumed that $\boldsymbol{\alpha} \sim \mathcal{CN}(0, \gamma^2\boldsymbol{\Sigma}_t)$. The parameters involved in the simulations are listed in Table I, including both the nominal and the actual target angle and incremental range.

Two benchmark detectors (devised assuming a perfect knowledge of $\boldsymbol{H}$ and resorting to the GLRT and 2SGLRT decision statistics, respectively) are considered for comparison purposes, i.e.,

$$\begin{aligned} &\Lambda_{\mathrm{ben-GLRT}}(u,\delta) = \\ &\frac{1}{1+\boldsymbol{r}^{\dagger}\boldsymbol{S}^{-1}\boldsymbol{r}}\boldsymbol{r}^{\dagger}\boldsymbol{S}^{-1}\boldsymbol{H}\left[\boldsymbol{H}^{\dagger}\boldsymbol{S}^{-1}\boldsymbol{H}\right]^{-1}\boldsymbol{H}^{\dagger}\boldsymbol{S}^{-1}\boldsymbol{r} \end{aligned} \tag{50}$$

and

$$\Lambda_{\mathrm{ben-2SGLRT}}(u,\delta) = \boldsymbol{r}^{\dagger}\boldsymbol{S}^{-1}\boldsymbol{H}\left[\boldsymbol{H}^{\dagger}\boldsymbol{S}^{-1}\boldsymbol{H}\right]^{-1}\boldsymbol{H}^{\dagger}\boldsymbol{S}^{-1}\boldsymbol{r}. \tag{51}$$

Besides, two additional decision strategies, respectively based on the GLRT and 2SGLRT criteria and using the nominal values of u and δ (thus referred to as mismatched detectors), i.e.,

$$\begin{aligned} &\Lambda_{\mathrm{mis-GLRT}}(\bar{u},\bar{\delta}) = \\ &\frac{1}{1+\boldsymbol{r}^{\dagger}\boldsymbol{S}^{-1}\boldsymbol{r}}\boldsymbol{r}^{\dagger}\boldsymbol{S}^{-1}\bar{\boldsymbol{H}}\left[\bar{\boldsymbol{H}}^{\dagger}\boldsymbol{S}^{-1}\bar{\boldsymbol{H}}\right]^{-1}\bar{\boldsymbol{H}}^{\dagger}\boldsymbol{S}^{-1}\boldsymbol{r} \end{aligned} \tag{52}$$

and

$$\Lambda_{\mathrm{mis-2SGLRT}}(\bar{u},\bar{\delta}) = \boldsymbol{r}^{\dagger}\boldsymbol{S}^{-1}\bar{\boldsymbol{H}}\left[\bar{\boldsymbol{H}}^{\dagger}\boldsymbol{S}^{-1}\bar{\boldsymbol{H}}\right]^{-1}\bar{\boldsymbol{H}}^{\dagger}\boldsymbol{S}^{-1}\boldsymbol{r}. \tag{53}$$

are also included. Moreover, the single polarization (SP) counterparts of (50), (51), (52), and (53), exploiting the data received by the HH channels, are also reported. Their decision statistics are respectively given by

$$\Lambda_{\mathrm{ben-GLRT-SP}} = \frac{\left|\mathbf{s}^{\dagger}\left(u,\delta\right)\mathbf{S}^{-1}\mathbf{r}\right|^2}{\left(1+\mathbf{r}^{\dagger}\mathbf{S}^{-1}\mathbf{r}\right)\mathbf{s}^{\dagger}\left(u,\delta\right)\mathbf{S}^{-1}\mathbf{s}\left(u,\delta\right)}, \tag{54}$$

This article has been accepted for publication in IEEE Transactions on Aerospace and Electronic Systems. This is the author's version which has not been fully edited and content may change prior to final publication. Citation information: DOI 10.1109/TAES.2022.3210887

TABLE I: Simulation Parameters of the FDA-MIMO Radar

Parameter	Value	Parameter	Value
transmit elements M	4	receive elements N	10
bandwidth B	1 MHz	frequency increment Δf	0.5 MHz
angle of the target u	$\frac{0.891}{2(N+M)}$	incremental range of the target δ	$0.6\frac{\Delta f}{2B}$
nominal angle of the target $\bar{u}$	0	nominal incremental range of the target $\bar{\delta}$	0
target polarimetric parameter ϵ_t	0.28	target polarimetric parameter δ_t	1

$$\Lambda_{\text{ben}-\text{2SGLRT}-\text{SP}} = \frac{\left|\mathbf{s}^{\dagger}\left(u,\delta\right)\mathbf{S}^{-1}\mathbf{r}\right|^2}{\mathbf{s}^{\dagger}\left(u,\delta\right)\mathbf{S}^{-1}\mathbf{s}\left(u,\delta\right)}, \tag{55}$$

$$\Lambda_{\text{mis}-\text{GLRT}-\text{SP}} = \frac{\left|\mathbf{s}^{\dagger}\left(\bar{u},\bar{\delta}\right)\mathbf{S}^{-1}\mathbf{r}\right|^2}{\left(1+\mathbf{r}^{\dagger}\mathbf{S}^{-1}\mathbf{r}\right)\mathbf{s}^{\dagger}\left(\bar{u},\bar{\delta}\right)\mathbf{S}^{-1}\mathbf{s}\left(\bar{u},\bar{\delta}\right)}, \tag{56}$$

and

$$\Lambda_{\text{mis}-\text{2SGLRT}-\text{SP}} = \frac{\left|\mathbf{s}^{\dagger}\left(\bar{u},\bar{\delta}\right)\mathbf{S}^{-1}\mathbf{r}\right|^2}{\mathbf{s}^{\dagger}\left(\bar{u},\bar{\delta}\right)\mathbf{S}^{-1}\mathbf{s}\left(\bar{u},\bar{\delta}\right)}. \tag{57}$$

In the considered simulations, the parameters ε_1, ε_2, and ε_3, involved in **Algorithms 1, 2**, and **3**, respectively, are set as $\varepsilon_1 = \varepsilon_2 = \varepsilon_3 = 10^{-4}$. For **Algorithm 2**, $s = 1, \beta = 0.5, \zeta = 0.5$, whereas for **Algorithm 3**, $N_u = N_\delta = 250$. Additionally, 9 initial points $(\bar{u}, \bar{\delta})$, picked up within the constraint set $\mathcal{C}$, i.e., $\{-1/2, 0, 1/2\} \times \{-\frac{\Delta f}{2B}, 0, \frac{\Delta f}{2B}\}$ are used for the execution of the algorithms[7]. Then, the best achieved estimate in likelihood sense is selected.

In the reported simulations, three different interference scenarios are examined. In the first one, the useful signal is buried in white Gaussian noise; in the last two, clutter disturbance is considered.

1) White noise interference case: Figs. 3(a) and 3(b) show the P_d curves of the proposed detectors (assuming $K = 320$ secondary data) in a scenario dominated by white Gaussian noise, i.e., with the covariance matrix modeled as

$$\boldsymbol{M} = \sigma_n^2 \boldsymbol{I} \in \mathbb{H}^{2MN}, \tag{58}$$

where, without loss of generality, the noise power level σ_n^2 is assumed to be 0 dB.

Inspection of the figures highlights that the LAM detectors achieve the best performance, with a loss w.r.t. the benchmarks of almost 1 dB at $P_d = 0.9$. Furthermore, the GPM and CD methods exhibit nearly an identical behavior, with a gap smaller than 1 dB when compared with the LAM curve. The results confirm both the capabilities of the considered linearization technique to approximate the actual steering vector correctly and of the iterative ascent algorithms to provide close-to-optimum solutions to the optimization problem (21). A clear performance advantage over the mismatched detectors (which rely on the nominal parameters to derive the decision statistics) is highlighted, corroborating the effectiveness of the proposed strategies. The plots also reveal that, at $P_d = 0.9$, the benchmark SP detectors experience a performance degradation w.r.t. the full polarized counterparts of 7 dB for the GLRT-based detector and of 5 dB for the 2SGLRT one, pinpointing the advantage of the devised architectures to leverage the polarimetric diversity. Finally, a direct comparison between Figs. 3(a) and 3(b) does not reveal significant performance differences between the GLRT and 2SGLRT methodologies.

2) Clutter interference case: In this situation, the useful target echo return is assumed buried in clutter plus noise, with covariance matrix $\boldsymbol{M} \in \mathbb{H}^{2MN}$ modeled as

$$\boldsymbol{M} = \sigma_c^2 \boldsymbol{\Sigma}_c \otimes \boldsymbol{M}_c + \sigma_n^2 \boldsymbol{I}, \tag{59}$$

where σ_c^2 is the clutter power level, $\boldsymbol{M}_c \in \mathbb{C}^{MN \times MN}$ is an exponentially-shaped matrix with 1-lag correlation coefficient ρ_c accounting for the covariance between the returns from the same polarimetric channel, and $\boldsymbol{\Sigma}_c = \begin{bmatrix} 1 & \epsilon_c\sqrt{\delta_c} \\ \epsilon_c^*\sqrt{\delta_c} & \delta_c \end{bmatrix} \in \mathbb{C}^{2\times 2}$ indicates the clutter normalized polarimetric scattering matrix. Besides, without loss of generality $\sigma_n^2 = 0$ dB is assumed and a Clutter to Noise Ratio (CNR), i.e., $\text{CNR} = \sigma_c^2/\sigma_n^2$, of 30 dB is considered. Typical values of ϵ_c and δ_c for different clutter models are summarized in Table II (see also [1, 9, 52]).

The detection performance for two different clutter environments and a sample support size of $K = 320$ are reported in Figs. 4, 5, and 6. Specifically, assuming $\rho_c = 0.4$ and mixed clutter (see Table II), the P_d versus SINR curves of the GLRT-based detectors are displayed in Fig. 4(a), whereas the 2SGLRT counterparts are given in Fig. 4(b). The results show that the proposed adaptive techniques achieve almost the same detection performance in the high SINR regime, with a degradation, w.r.t. the benchmarks, of 1 dB at $P_d = 0.9$. Precisely, the LAM-based and GPM-based detectors almost achieve the same (and closest to the optimum) performance, with a very slight advantage over the CD counterparts. This behavior represents a first confirmation of the effectiveness of the considered techniques to handle a challenging clutter-dominated scenario. On the contrary, the mismatched detectors exhibit a clear performance degradation w.r.t. the benchmarks, with a gap between the curves in the order of 6 dB. A further inspection of the figures also highlights that, for this challenging scenario, the SP detectors are not able to provide an adequate detection performance, further corroborating the need to devise appropriate detection strategies leveraging the polarimetric diversity techniques.

In Fig. 5, the same scenario as Fig. 4 but for $\rho_c = 0.9$, is considered. Inspection of the figure reveals that the proposed detectors achieve almost the same performance. Nonetheless, the mismatched detectors exhibit a noticeable performance degradation in a clutter environment with $\rho = 0.9$ w.r.t. the $\rho = 0.4$ case, especially with reference to the GLRT configuration. In this regard, it is worth analyzing the similarity θ_{sim} between the true and the nominal array steering

[7]It is worth noting that several feasible initial vectors can be employed for the execution of the algorithms to minimize the risk of being trapped in a local maximum.

This article has been accepted for publication in IEEE Transactions on Aerospace and Electronic Systems. This is the author's version which has not been fully edited and content may change prior to final publication. Citation information: DOI 10.1109/TAES.2022.3210887

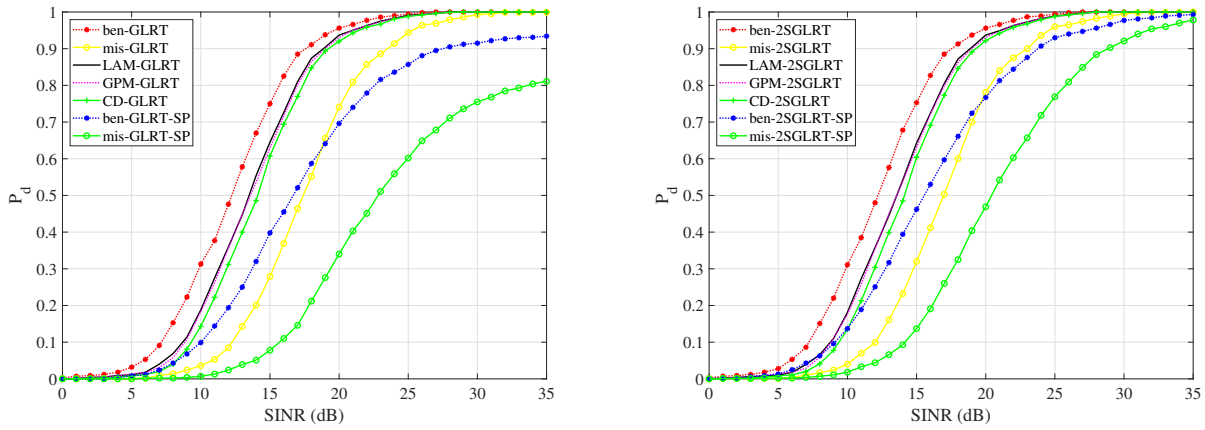

Fig. 4: Detection performance for a mixed clutter environment (see Table II) with $\rho_c = 0.4$, assuming $K = 320$ and the parameters of Table I. Fig. (a) considers the GLRT-based detectors, whereas Fig. (b) reports the 2SGLRT counterparts.

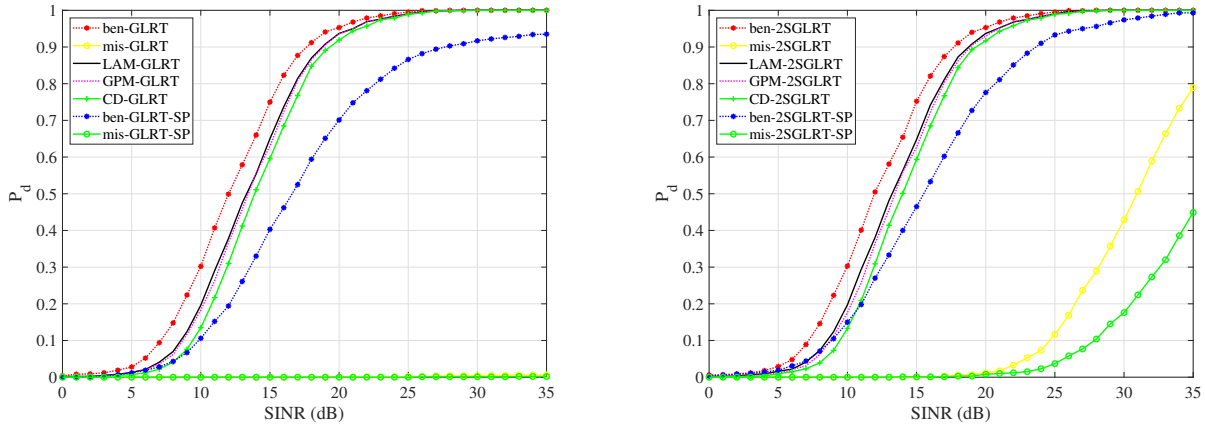

Fig. 5: Detection performance for a mixed clutter environment (see Table II) with $\rho_c = 0.9$, assuming $K = 320$ and the parameters of Table I. Fig. (a) considers the GLRT-based detectors, whereas Fig. (b) reports the 2SGLRT counterparts.

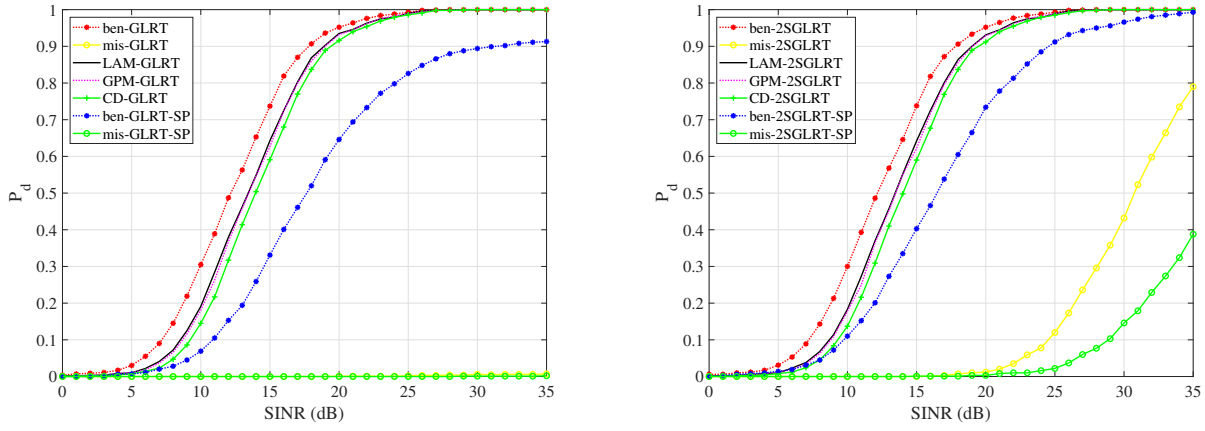

Fig. 6: Detection performance for a clutter trees environment (see Table II) with $\rho_c = 0.9$, assuming $K = 320$ and the parameters of Table I. Fig. (a) considers the GLRT-based detectors, whereas Fig. (b) reports the 2SGLRT counterparts.

TABLE II: Typical parameters for polarimetric clutter characterization [9]

Clutter Models	δ_c	ϵ_c	ρ_c
Trees	0.89	0.64	0.9
Mixed	1.08	0.57	0.9

matrices,measured as

$$\theta_{\text{sim}} = \frac{|\text{tr}(\breve{\boldsymbol{H}}_t{}^{\dagger}\breve{\boldsymbol{H}}))|}{\sqrt{\text{tr}(\breve{\boldsymbol{H}}_t{}^{\dagger}\breve{\boldsymbol{H}}_t)}\sqrt{\text{tr}(\breve{\boldsymbol{H}}^{\dagger}\breve{\boldsymbol{H}})}}, \tag{60}$$

with $\breve{\boldsymbol{H}}_t = \boldsymbol{M}^{-1/2}\boldsymbol{H}(u,\delta)$ and $\breve{\boldsymbol{H}} = \boldsymbol{M}^{-1/2}\boldsymbol{H}(\bar{u},\bar{\delta})$. Specifically, for the case of $\rho = 0.4$, the similarity is $\theta_{\text{sim}} = 0.5715$, whereas for the $\rho = 0.9$ scenario, $\theta_{\text{sim}} = 0.0930$, which corroborates the larger performance loss experienced by the mismatched detectors in the latter scenario w.r.t. the former one.

In Fig. 6 an additional clutter model, i.e., clutter from trees (whose parameters are reported in Table II) with $\rho_c = 0.9$ is considered for the interference simulation. Analysis of the curves highlights the absence of noticeable differences when compared with the mixed clutter case of Fig. 5.

In Fig. 7, the performance of the detectors is compared for different sample support sizes in a scenario of mixed clutter interference with $\rho_c = 0.9$. In this regard, Figs. 7(a), 7(c), and 7(e) report the performance of the GLRT-based detectors, whereas Figs. 7(b), 7(d), and 7(f) those related to the 2SGLRT-based strategies. Specifically, assuming $K = 320$, $K = 240$, and $K = 120$ secondary data to estimate the covariance matrix, the case of LAM-based detectors is displayed in Figs. 7(a) and 7(b), that of the GPM-based strategies in Figs. 7(c) and 7(d), and the situation related to the CD-based detectors is analyzed in Figs. 7(e) and 7(f). As expected, capitalizing on a larger number of secondary data leads to a clear performance gain, owing to a better estimate of the covariance matrix. Remarkably, even with a reduced sample support size, the performance loss between the proposed receivers and the corresponding benchmarks (either with $K = 320$, $K = 240$, or $K = 120$) remains almost acceptable, with a gap smaller than 2 dB for $P_d = 0.9$, for all the considered architectures. Besides, regardless of the number of secondary data, all the proposed detectors achieve a better detection performance than the SP benchmarks, stressing again the benefit of the polarimetric domain.

To summarize, the detectors based on either the LAM or GPM procedures provide the best solutions (in terms of P_d for a given P_{fa}) to the target detection problem for all the analyzed case studies. Additionally, the proposed methods exhibit substantially the same computational complexity provided the number of iterations is small enough.

VI. Conclusion

This paper has considered the design of adaptive detectors for a polarimetric FDA-MIMO radar in a scenario characterized by the presence of interference with unknown spectral properties. The detection problem, formulated in terms of a binary hypothesis test, has been handled by resorting either to the GLRT or to the 2SGLRT criterion, demanding the ML estimation of the interference covariance matrix and, under the H_1 hypothesis, also of the unknown target parameters. To get computationally efficient even though sub-optimal solutions to the resulting optimization problem, three iterative strategies have been proposed. First, a procedure has been developed leveraging a LAM technique, which capitalizes on the target location offsets w.r.t. the nominal array steering. Then, a GPM technique has been considered, that iteratively updates the parameters according to the gradient of the objective function. Finally, a CD approach has been investigated, which sequentially optimizes one variable while keeping the other fixed. Noticeably, the proposed detectors ensure the so-called bounded CFAR property. At the analysis stage, the performance of the receivers has been numerically assessed also in comparisons with benchmarks. The results, for both white and clutter interference (either mixed or trees), have pinpointed the effectiveness of the devised architectures to provide a detection performance close to the clairvoyant structure. Furthermore, a clear performance advantage over both mismatched detectors and the single polarization counterparts has been underlined, corroborating the strength of the proposed detectors.

Future research studies might include the design of additional decision strategies according to other sub-optimal criteria, e.g., Rao [53] and Wald [54] tests, as well as the extension of the framework to different scenarios such as compound Gaussian disturbance [55], structured interference covariance matrix, as well as the case of extended targets occupying multiple range cells.

Appendix

A. Expressions for $\boldsymbol{H}_u$ and $\boldsymbol{H}_\delta$

Denoting by $\boldsymbol{s}_u \in \mathbb{C}^{MN}$ and $\boldsymbol{s}_\delta \in \mathbb{C}^{MN}$ the derivative functions of $\boldsymbol{s}(u,\delta)$ w.r.t. u and δ, respectively, they are given by [23]

$$\begin{aligned}\boldsymbol{s}_u = \frac{\partial \boldsymbol{s}(u,\delta)}{\partial u} = \frac{\partial \boldsymbol{b}(u)}{\partial u} \otimes [\boldsymbol{c}(u) \odot \boldsymbol{a}(\delta)] \\ + \boldsymbol{b}(u) \otimes \left[\frac{\partial \boldsymbol{c}(u)}{\partial u} \odot \boldsymbol{a}(\delta)\right]\end{aligned} \tag{61}$$

and

$$\boldsymbol{s}_\delta = \frac{\partial \boldsymbol{s}(u,\delta)}{\partial \delta} = \boldsymbol{b}(u) \otimes \left[\boldsymbol{c}(u) \odot \frac{\partial \boldsymbol{a}(\delta)}{\partial \delta}\right], \tag{62}$$

where

- $\frac{\partial \boldsymbol{b}(u)}{\partial u} = j2\pi\frac{d}{\lambda_0}\boldsymbol{E}_T\boldsymbol{b}(u)$;
- $\frac{\partial \boldsymbol{c}(u)}{\partial u} = j2\pi\frac{d}{\lambda_0}\boldsymbol{R}^{\text{T}}\boldsymbol{E}_R\boldsymbol{d}(u)$;
- $\frac{\partial \boldsymbol{a}(\delta)}{\partial \delta} = j\pi\boldsymbol{E}_R\boldsymbol{a}(\delta)$.

with

- $\boldsymbol{E}_T = \text{diag}\left([0,1,...,N-1]^{\text{T}}\right) \in \mathbb{R}^{N\times N}$;
- $\boldsymbol{E}_R = \text{diag}\left([0,1,...,M-1]^{\text{T}}\right) \in \mathbb{R}^{M\times M}$.

Therefore,

$$\boldsymbol{H}_u = \begin{bmatrix} \boldsymbol{s}_u & \boldsymbol{0} \\ \boldsymbol{0} & \boldsymbol{s}_u \end{bmatrix} \tag{63}$$

and

$$\boldsymbol{H}_\delta = \begin{bmatrix} \boldsymbol{s}_\delta & \boldsymbol{0} \\ \boldsymbol{0} & \boldsymbol{s}_\delta \end{bmatrix}, \tag{64}$$

This article has been accepted for publication in IEEE Transactions on Aerospace and Electronic Systems. This is the author's version which has not been fully edited and content may change prior to final publication. Citation information: DOI 10.1109/TAES.2022.3210887

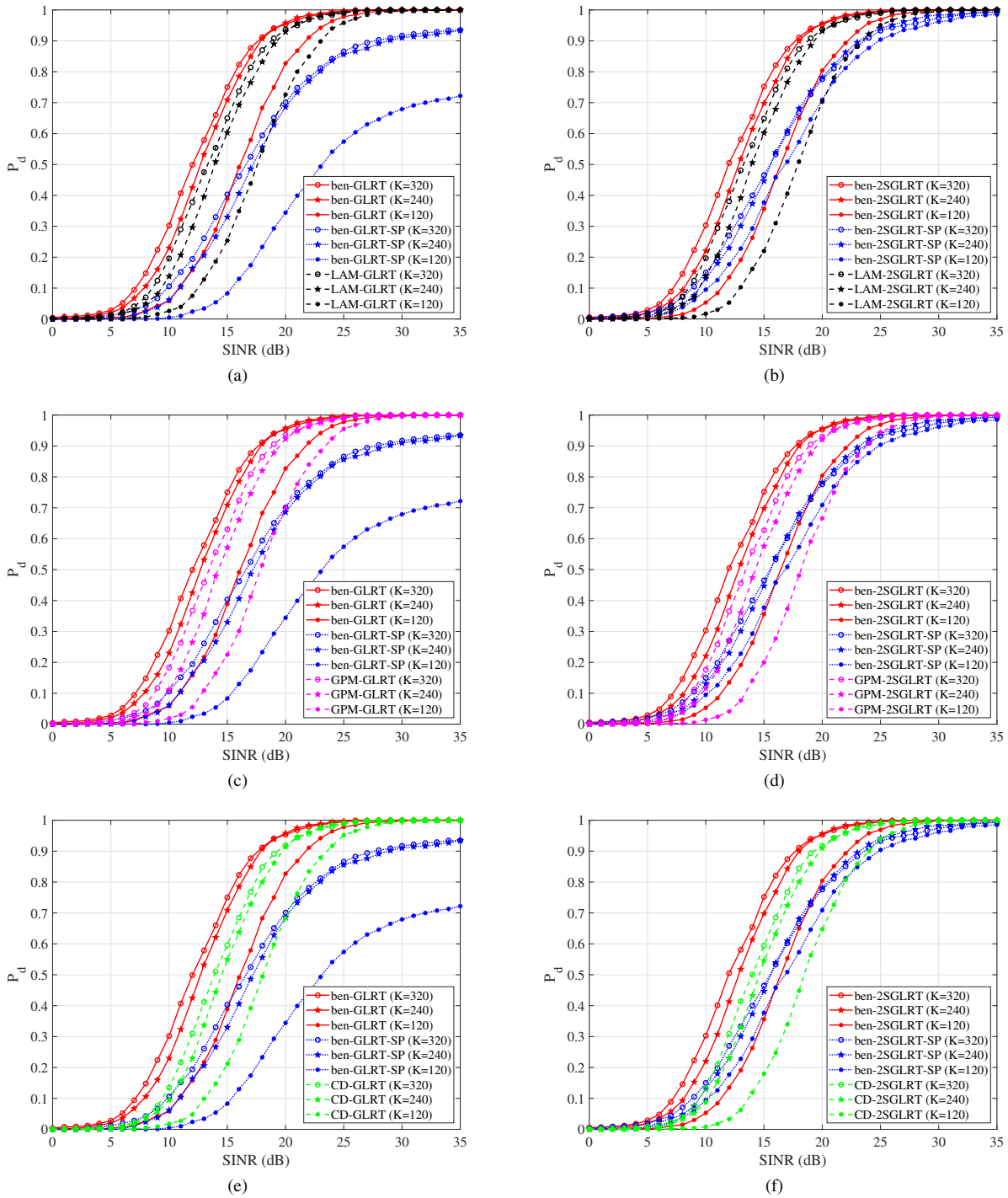

Fig. 7: Detection performance of the LAM, GPM, and CD methods for different sample support sizes, i.e., $K = 320$, $K = 240$, $K = 120$, assuming a mixed clutter environment (see Table II) with $\rho_c = 0.9$ and the parameters of Table I. Figs. (a), (c), and (d) report the performance of the GLRT-based decision statistics; Figs. (b), (d), and (f) that of the 2SGLRT rules.

B. Proof of Proposition 1

Proof: The existence of the global minimizer of (30) is guaranteed by the Weierstrass theorem [35], being the objective function (30) continuous and the feasible set $\mathcal{C}$ non-empty and compact. Besides, the stationary points of the objective function in (30) are obtained by nulling the objective gradient, namely by solving the equation

$$\nabla_{\Delta\boldsymbol{\theta}}\left[(\hat{\boldsymbol{r}}-\hat{\boldsymbol{H}}\Delta\boldsymbol{\theta})^{\dagger}(\hat{\boldsymbol{r}}-\hat{\boldsymbol{H}}\Delta\boldsymbol{\theta})\right]=0. \tag{65}$$

After some algebra, equation (65) can be expressed as

$$\Re\{\hat{\boldsymbol{H}}^{\dagger}\hat{\boldsymbol{r}}\}-\Re\{\hat{\boldsymbol{H}}^{\dagger}\hat{\boldsymbol{H}}\}\Delta\boldsymbol{\theta}=0, \tag{66}$$

meaning that the unique stationary point is obtained as

$$\Delta\boldsymbol{\theta}_1=\left[\Re\{\hat{\boldsymbol{H}}^{\dagger}\hat{\boldsymbol{H}}\}\right]^{-1}\Re\{\hat{\boldsymbol{H}}^{\dagger}\hat{\boldsymbol{r}}\}. \tag{67}$$

Remarkably, if it is feasible, i.e., $\Delta\boldsymbol{\theta}_1\in\mathcal{C}$, it is the optimal solution to the optimization problem (30). Otherwise, an optimal solution can be found restricting the objective function to the boundaries of $\mathcal{C}$ and determining, for each edge, the corresponding minimizer.

Case A: *Left and right edges* ($\Delta u=\pm\kappa$).

Denoting by $\hat{\boldsymbol{r}}_{\pm\kappa}=\hat{\boldsymbol{r}}-\hat{\boldsymbol{h}}_u(\pm\kappa)$, the optimization problem (30), restricted to $\Delta u=\pm\kappa$, boils down to

$$\min_{|\Delta\delta|\leq\rho}(\hat{\boldsymbol{r}}_{\pm\kappa}-\hat{\boldsymbol{H}}_{\delta}\Delta\delta)^{\dagger}(\hat{\boldsymbol{r}}_{\pm\kappa}-\hat{\boldsymbol{H}}_{\delta}\Delta\delta). \tag{68}$$

The objective function of (68) can be written as

$$a'\,\Delta\delta^2-2b'_{\pm\kappa}\,\Delta\delta+c'_{\pm\kappa}, \tag{69}$$

where

$$a'=\|\hat{\boldsymbol{H}}_{\delta}\|^2, \tag{70a}$$

$$b'_{\pm\kappa}=\Re\{\hat{\boldsymbol{r}}^{\dagger}_{\pm\kappa}\hat{\boldsymbol{h}}_{\delta}\}, \tag{70b}$$

$$c'_{\pm\kappa}=\|\hat{\boldsymbol{r}}_{\pm\kappa}\|^2. \tag{70c}$$

Since $a'>0$, (68) is a convex optimization problem, whose optimal solution is given by

$$\Delta\delta^*_{\pm}=\min(\rho,\max(b'_{\pm\kappa}/a',-\rho)). \tag{71}$$

Therefore, the two candidate optimal solutions associated with the right and left edges are given by

$$\Delta\boldsymbol{\theta}_2=[\kappa,\Delta\delta^*_{+}] \tag{72}$$

and

$$\Delta\boldsymbol{\theta}_3=[-\kappa,\Delta\delta^*_{-}]. \tag{73}$$

Case B: *Upper and lower edges* ($\Delta\delta=\pm\rho$).

Similarly to the **Case A**, denoting by $\hat{\boldsymbol{r}}_{\pm\rho}=\hat{\boldsymbol{r}}-\hat{\boldsymbol{h}}_{\delta}(\pm\rho)$, the candidate optimal solutions associated with the superior and inferior edges are given by

$$\Delta\boldsymbol{\theta}_4=[\Delta u^*_{+},\rho] \tag{74}$$

and

$$\Delta\boldsymbol{\theta}_5=[\Delta u^*_{-},-\rho], \tag{75}$$

where

$$\Delta u^*_{\pm}=\min(\kappa,\max(b''_{\pm\rho}/a'',-\kappa)) \tag{76}$$

with

$$a''=\|\hat{\boldsymbol{h}}_u\|^2, \tag{77a}$$

$$b''_{\pm\rho}=\Re\{\hat{\boldsymbol{r}}^{\dagger}_{\pm\rho}\hat{\boldsymbol{h}}_u\}. \tag{77b}$$

As a consequence, an optimal solution to the optimization problem (30) is given by

$$\Delta\boldsymbol{\theta}^{(h)}=\underset{\Delta\boldsymbol{\theta}\in\{\Delta\boldsymbol{\theta}_i\}_{i=1}^{5}}{\arg\min}\;(\hat{\boldsymbol{r}}-\hat{\boldsymbol{H}}\Delta\boldsymbol{\theta})^{\dagger}(\hat{\boldsymbol{r}}-\hat{\boldsymbol{H}}\Delta\boldsymbol{\theta}). \tag{78}$$

■

C. Computation of $\boldsymbol{g}_{\triangle}(u,\delta)$

Denoting by $\bar{\boldsymbol{r}}=\boldsymbol{S}^{-\frac{1}{2}}\boldsymbol{r}\in\mathbb{C}^{2MN}$ and $\check{\boldsymbol{H}}=\boldsymbol{S}^{-\frac{1}{2}}\boldsymbol{H}\in\mathbb{C}^{2MN\times 2}$, $g(u,\delta)$ can be rewritten as

$$\begin{aligned}g(u,\delta)&=\bar{\boldsymbol{r}}^{\dagger}\check{\boldsymbol{H}}\left[\check{\boldsymbol{H}}^{\dagger}\check{\boldsymbol{H}}\right]^{-1}\check{\boldsymbol{H}}^{\dagger}\bar{\boldsymbol{r}}\\&=\bar{\boldsymbol{r}}^{\dagger}\bar{\boldsymbol{P}}_{\check{H}}\bar{\boldsymbol{r}}\end{aligned} \tag{79}$$

where $\bar{\boldsymbol{P}}_{\check{H}}=\check{\boldsymbol{H}}\left[\check{\boldsymbol{H}}^{\dagger}\check{\boldsymbol{H}}\right]^{-1}\check{\boldsymbol{H}}^{\dagger}\in\mathbb{C}^{2MN\times 2MN}$.

Therefore, the first derivatives of $g(u,\delta)$ w.r.t. u and δ, are given by [Eq. A.394, [56]]

$$\frac{\partial g(u,\delta)}{\partial x}=\bar{\boldsymbol{r}}^{\dagger}\frac{\partial\bar{\boldsymbol{P}}_{\check{H}}}{\partial x}\bar{\boldsymbol{r}}\;,x\in\{u,\delta\}, \tag{80}$$

where

- $\frac{\partial\bar{\boldsymbol{P}}_{\check{H}}}{\partial x}=\bar{\boldsymbol{P}}^{\perp}_{\check{H}}\check{\boldsymbol{H}}_x\check{\boldsymbol{H}}^{\dagger}+\left(\bar{\boldsymbol{P}}^{\perp}_{\check{H}}\check{\boldsymbol{H}}_x\check{\boldsymbol{H}}^{\dagger}\right)^{\dagger}$ with $\check{\boldsymbol{H}}_x=\boldsymbol{S}^{-1/2}\boldsymbol{H}_x\in\mathbb{C}^{2MN\times 2},x\in u,\delta$;
- $\bar{\boldsymbol{P}}^{\perp}_{\check{H}}=\boldsymbol{I}-\bar{\boldsymbol{P}}_{\check{H}}\in\mathbb{C}^{2MN\times 2MN}$.

As a consequence, the gradient of $g(u,\delta)$ is given by

$$\boldsymbol{g}_{\triangle}(u,\delta)=\left[\frac{\partial g(u,\delta)}{\partial u},\frac{\partial g(u,\delta)}{\partial\delta}\right]^{\mathrm{T}}. \tag{81}$$

D. Proof of $g(u,\delta)\in C^{1,1}_L$

Before proceeding with the proof, let us first introduce the following lemma [34], which provides a sufficient condition for a function to be in $C^{1,1}_L$.

Lemma A.1: Let $f(\boldsymbol{x})$ belongs to C^2 with $\boldsymbol{f}_{\triangle\triangle}(\boldsymbol{x})$ its Hessian matrix; if there exists $L>0$ such that $\|\boldsymbol{f}_{\triangle\triangle}(\boldsymbol{x})\|\leq L$ holds true for any $\boldsymbol{x}\in\mathbb{R}^n$, then $f(\boldsymbol{x})\in C^{1,1}_L$. ■

Therefore, in order to exploit the above result, in the following, the function $g(u,\delta)$ is proved to fulfill the conditions required by *Lemma A.1*. To this end, let us report again, for easy of reference, the detailed expression of $\boldsymbol{s}(u,\delta)$, i.e.,

$$\boldsymbol{s}(u,\delta)=\boldsymbol{b}(u)\otimes[\boldsymbol{c}(u)\odot\boldsymbol{a}(\delta)]\in\mathbb{C}^{MN} \tag{82}$$

with

$$\boldsymbol{b}(u)=\left[1,e^{j2\pi\frac{d}{\lambda_0}u},\ldots,e^{j2\pi\frac{d}{\lambda_0}(N-1)u}\right]^{\mathrm{T}}\in\mathbb{C}^{N}, \tag{83a}$$

$$\boldsymbol{c}(u)=\boldsymbol{R}^{\mathrm{T}}\boldsymbol{d}(u)\in\mathbb{C}^{M}, \tag{83b}$$

$$\boldsymbol{d}(u)=\left[1,e^{j2\pi\frac{d}{\lambda_0}u},\ldots,e^{j2\pi\frac{d}{\lambda_0}(M-1)u}\right]^{\mathrm{T}}\in\mathbb{C}^{M}, \tag{83c}$$

$$\boldsymbol{a}(\delta)=\left[1,e^{j\pi\delta}\ldots,e^{j\pi(M-1)\delta}\right]^{\mathrm{T}}\in\mathbb{C}^{M}. \tag{83d}$$

From equations (83), it is straightforward to see that $\boldsymbol{b}(u)$, $\boldsymbol{c}(u)$, $\boldsymbol{d}(u)$, and $\boldsymbol{a}(\delta)$ belong to C^2 and hence $\boldsymbol{s}(u,\delta)$ belongs

to C^2. Therefore, assuming $\boldsymbol{S} \succ 0$, which occurs almost surely being $K \geq 2MN$,

$$g(u,\delta) = \boldsymbol{r}^\dagger \boldsymbol{S}^{-1}\boldsymbol{H}\left[\boldsymbol{H}^\dagger \boldsymbol{S}^{-1}\boldsymbol{H}\right]^{-1}\boldsymbol{H}^\dagger \boldsymbol{S}^{-1}\boldsymbol{r} \tag{84}$$

belongs to C^2 since

$$\boldsymbol{H} = \boldsymbol{H}(u,\delta) = \begin{bmatrix} \mathbf{s}(u,\delta) & \mathbf{0} \\ \mathbf{0} & \mathbf{s}(u,\delta) \end{bmatrix} \in \mathbb{C}^{2MN\times 2} \tag{85}$$

belongs to C^2 and it is full rank.

Then, it can be verified that $\|\boldsymbol{g}_{\triangle\triangle}(u,\delta)\|$ is continuous and periodic, with

$$\boldsymbol{g}_{\triangle\triangle} = \begin{bmatrix} g_{uu}(u,\delta) & g_{u\delta}(u,\delta) \\ g_{\delta u}(u,\delta) & g_{\delta\delta}(u,\delta) \end{bmatrix},$$

since $\|\boldsymbol{A}\|$ is a continuous function w.r.t. $\boldsymbol{A} \in \mathbb{H}^N$ and the second derivatives of $g(u,\delta)$, i.e., $g_{xy}(u,\delta), x, y \in \{u,\delta\}$ are continuous and periodic functions with period $T_u = \lambda_0/d$ and $T_\delta = 2$ along u and δ directions, respectively (see Appendix E). Therefore, invoking the Weierstrass theorem [35],

$$\|\boldsymbol{g}_{\triangle\triangle}(u,\delta)\| \leq \max_{u\in[0,T_u],\delta\in[0,T_\delta]} \|\boldsymbol{g}_{\triangle\triangle}(u,\delta)\| = L < \infty. \tag{86}$$

E. Proof that the second derivatives of $g(u,\delta)$ are periodic functions

This Appendix is composed of two parts: first, $\boldsymbol{s}(u,\delta)$ and $g(u,\delta)$ are proved to be periodic functions. Then, the periodicity of the first and second order derivatives of $g(u,\delta)$ is analyzed.

From equations (83), it is easy to verify that $\boldsymbol{s}(u,\delta)$ is a periodic function with period T_u and T_δ along u and δ directions, respectively, being

- $\boldsymbol{b}(u)$ periodic with period T_u;
- $\boldsymbol{d}(u)$ and $\boldsymbol{c}(u)$ periodic with period T_u;
- $\boldsymbol{a}(\delta)$ periodic with period T_δ.

As a consequence, $g(u,\delta)$ shares the same periodicity as $\boldsymbol{s}(u,\delta)$.

Now, the periodicity of the first and second order derivatives can be established resorting to the following lemma.

Lemma A.2: Let $f(x,y) : \mathbb{R}^2 \to \mathbb{R}$ be a continuous, derivable, and periodic function with period T_x and T_y along the x and y directions, respectively. Then, $f_x(x,y) = \frac{\partial f(x,y)}{\partial x}$ and $f_y(x,y) = \frac{\partial f(x,y)}{\partial y}$ are periodic functions with the same periodicities as $f(x,y)$.

Proof: Denoting by $x_1 = x + N_1 T_x$ and $y_1 = y + N_2 T_y$, with $N_1, N_2 \in \mathbb{N}$,

$$\begin{aligned} f_x(x_1,y_1) &= f_x(x+N_1T_x, y+N_2T_y) \\ &= \lim_{h\to 0} \frac{f(x+N_1T_x+h, y+N_2T_y) - f(x+N_1T_x, y+N_2T_y)}{h} \\ &= \lim_{h\to 0} \frac{f(x+h,y)-f(x,y)}{h} = f_x(x,y). \end{aligned}$$

Therefore, $f_x(x,y)$ is periodic as $f(x,y)$. Along the same line, it is straightforward to prove that $f_y(x,y)$ shares the same periodicity as $f(x,y)$. ∎

Exploiting the above result, $g_u(u,\delta)$ and $g_\delta(u,\delta)$ are periodic functions with the same period as $g(u,\delta)$. Then, resorting again to Lemma A.2, $g_{uu}(u,\delta)$ and $g_{u\delta}(u,\delta)$, as well as $g_{\delta u}(u,\delta)$ and $g_{\delta\delta}(u,\delta)$, share the same periodicity as $g_u(u,\delta)$ and $g_\delta(u,\delta)$, respectively. As a result, the first and second order derivatives of $g(u,\delta)$ are periodic functions as $g(u,\delta)$.

REFERENCES

[1] L. M. Novak, M. B. Novak, and M. J. Cardullo, "Studies of target detection algorithms that use polarimetric radar data," *IEEE Trans. Aerosp. Electron. Syst.*, vol. 25, no. 2, pp. 150-165, 1989.

[2] A. De Maio and G. Ricci, "A polarimetric adaptive matched filter," *Signal Process.*, vol. 81, no. 12, pp. 2583-2589, 2001.

[3] G. Alfano, A. De Maio, and E. Conte, "Polarization diversity detection of distributed targets in compound-Gaussian Clutter," *IEEE Trans. Aerosp. Electron. Syst.*, vol. 40, no. 2, pp. 755-765, 2004.

[4] A. Nehorai and E. Paldi, "Vector-sensor array processing for electromagnetic source localization," *IEEE Trans. Signal Process.*, vol. 42, no. 2, pp. 376-398, 1994.

[5] Y. Wang, W. Xia, Z. He, H. Li, and A. P. Petropulu, "Polarimetric detection in compound Gaussian clutter with Kronecker structured covariance matrix," *IEEE Trans. Signal Process.*, vol. 65, no. 17, pp. 4562-4576, 2017.

[6] H. Park, J. Li, and H. Wang, "Polarization-space-time domain generalized likelihood ratio detection of radar targets," *Signal Process.*, vol. 41, no. 2, pp. 153-164, 1995.

[7] D. Pastina, P. Lombardo and T. Bucciarelli, "Adaptive polarimetric target detection with coherent radar Part I: detection against Gaussian background", *IEEE Trans. Aerosp. Electron. Syst.*, vol. 37, no. 4, pp. 1194-1206, 2001.

[8] C. Hao, S. Gazor, X. Ma, S. Yan, C. Hou, and D. Orlando, "Polarimetric detection and range estimation of a point-like target," *IEEE Trans. Aerosp. Electron. Syst.*, vol. 52, no. 2, pp. 603-616, 2016.

[9] A. De Maio and G. Alfano, "Polarimetric adaptive detection in non-Gaussian noise," *Signal Process.*, vol. 83, no. 2, pp. 297-306, 2003.

[10] Y. Yang, S. P. Xiao, X. S. Wang, W. M. Zhang, and Y. Z. Li, "Generalised polarimetric whitening filter for polarimetric MIMO radar detection," *IET Radar Sonar Navig.*, vol. 13, no. 1, pp. 1-7, 2018.

[11] L. Shen, Z. Liu, and Y. Xu, "Polarimetric detection and range estimation for a point-like target in non-Gaussian clutter," *IET Radar Sonar Navig.*, vol. 12, no. 3, pp. 361-365, 2018.

[12] L. Kong, G. Cui, X. Yang, and J. Yang, "Rao and Wald tests design of polarimetric multiple-input multiple-output radar in compound-Gaussian clutter," *IET Signal Process.,* vol. 5, no. 1, pp. 85-96, 2011.

[13] A. De Maio, G. Alfano, and E. Conte, "Polarization diversity detection in compound-Gaussian clutter," *IEEE Trans. Aerosp. Electron. Syst.*, vol. 40, no. 1, pp. 114-131, 2004.

[14] W.-Q. Wang, "Frequency Diverse Array Antenna: New Opportunities," *IEEE Antennas and Propag. Magazine*, vol. 57, no. 2, pp. 145-152, 2015.

[15] A. Basit, W. Khan, S. Khan, and I. M. Qureshi, "Development of frequency diverse array radar technology: a review," *IET Radar Sonar Navig.*, vol. 12, no. 2, pp. 165-175, 2018.

[16] L. Lan, G. Liao, J. Xu, Y. Zhang, and B. Liao, "Transceive beam-forming with accurate nulling in FDA-MIMO radar for imaging," *IEEE Trans. Geosci. Remote Sens.*, vol. 58, no. 6, pp. 4145-4159, 2020.

[17] P. F. Sammartino, C. J. Baker, and H. D. Griffiths, "Frequency diverse MIMO techniques for radar," *IEEE Trans. Aerosp. Electron. Syst.*, vol. 49, no. 1, pp. 201-222, 2013.

[18] J. Xu, G. Liao, S. Zhu, L. Huang, and H. C. So, "Joint range and angle estimation using MIMO radar with frequency diverse array," *IEEE Trans. Signal Process.*, vol. 63, no. 13, pp. 3396-3410, 2015.

[19] S. Sedighi, B. Shankar, K. V. Mishra, and B. Ottersten, "Optimum Design for Sparse FDA-MIMO Automotive Radar," *2019 53rd Asilomar Conference on Signals, Systems, and Computers,* 2019, pp. 913-918.

[20] L. Lan, J. Xu, G. Liao, Y. Zhang, F. Fioranelli, and H. C. So, "Suppression of mainbeam deceptive jammer with FDA-MIMO radar," *IEEE Trans Vehic. Tech.*, vol. 69, no. 10, pp. 11584-11598, 2020.

[21] C. Cui, J. Xu, R. Gui, W. Wang, and W. Wu, "Search-Free DOD, DOA and Range Estimation for Bistatic FDA-MIMO Radar," *IEEE Access*, vol. 6, pp. 15431-15445, 2018.

[22] C. Wang, Z. Li, and X. Zhang, "FDA-MIMO for joint angle and range estimation: unfolded coprime framework and parameter estimation algorithm," *IET Radar, Sonar Navigation.*, vol. 14, no. 6, pp. 917-926, 2020.

[23] L. Lan, M. Rosamilia, A. Aubry, A. De Maio and G. Liao, "Single-Snapshot Angle and Incremental Range Estimation for FDA-MIMO Radar," *IEEE Trans. Aerosp. Electron. Syst.*, vol. 57, no. 6, pp. 3705-3718, 2021.

[24] S. Qin, Y. D. Zhang, M. G. Amin and F. Gini, "Frequency diverse coprime arrays with coprime frequency offsets for multitarget localization," *IEEE J. Sel. Topics Signal Process.,* vol. 11, no. 2, pp. 321-335, 2017.

[25] R. Roy and T. Kailath, "ESPRIT-estimation of signal parameters via rotational invariance techniques," *IEEE Trans. on Acoustics, Speech, and Signal Process.*, vol. 37, no. 7, pp. 984-995, 1989.

[26] J. Xiong, W. Wang, and K. Gao, "FDA-MIMO Radar Range-Angle Estimation: CRLB, MSE, and Resolution Analysis," *IEEE Trans. Aerosp. Electron. Syst.*, vol. 54, no. 1, pp. 284-294, 2018.

[27] Y. Zhu, L. Liu, Z. Lu, and S. Zhang, "Target Detection Performance Analysis of FDA-MIMO Radar," *IEEE Access*, vol. 7, pp. 164276-164285, 2019.

[28] B. Huang, A. Basit, R. Gui, and W. -Q. Wang, "Adaptive Moving Target Detection Without Training Data for FDA-MIMO Radar," *IEEE Trans Vehic. Tech.*, vol. 71, no. 1, pp. 220-232, Jan. 2022.

[29] B. Li, W. Bai, and G. Zheng, "Successive ESPRIT algorithm for joint DOA-range-polarization estimation with polarization sensitive FDA-MIMO radar," *IEEE Access*, vol. 6, pp. 36376-36382, 2018.

[30] J. Wang and S. Jiang, "Angle-polarization-range estimation using sparse polarization sensitive FDA-MIMO radar with coprime frequency offsets," *IEEE Access*, vol. 7, pp. 146759-146771, 2019.

[31] B. K. Chalise, Y. D. Zhang, and B. Himed, "Compressed sensing based joint DOA and polarization angle estimation for sparse arrays with dual-polarized antennas," *IEEE GlobalSIP 2018*, pp. 251-255, 2018.

[32] L. Lan, A. Marino, A. Aubry, A. De Maio, G. Liao, J. Xu, and Y. Zhang, "GLRT-Based Adaptive Target Detection in FDA-MIMO Radar," *IEEE Trans. Aerosp. Electron. Syst.*, vol. 57, no. 1, pp. 597-613, 2021.

[33] A. Aubry, A. De Maio, S. Marano, and M. Rosamilia, "Single-Pulse Simultaneous Target Detection and Angle Estimation in a Multichannel Phased Array Radar," *IEEE Trans. Signal Process.*, vol. 68, pp. 6649-6664, 2020.

[34] A. Beck, Introduction to nonlinear optimization: Theory, algorithms, and applications with MATLAB, Technion-Israel Institute of Technology, 2014.

[35] D. P. Bertsekas, Nonlinear programming, Athena Scientific, Belmont, Massachusetts, 1999.

[36] C. A. Balanis. Antenna theory-analysis and design. New York: Harper & Row Publishers, Inc., 1982.

[37] W. L. Melvin and J. Scheer, Principles of Modern Radar: Advanced techniques, vol. 2, IET Digital Library, 2012

[38] J. Li and R. T. Compton, "Angle and polarization estimation using ESPRIT with a polarization sensitive array," *IEEE Trans. on Antennas Propag.*, vol. 39, no. 9, pp. 1376-1383, 1991.

[39] R. C. Davis, L. E. Brennan, and L. S. Reed, "Angle Estimation with Adaptive Arrays in External Noise Fields," *IEEE Trans. Aerosp. Electron. Syst.*, vol. AES-12, no. 2, pp. 179-186, 1976.

[40] U. Nickel, "Monopulse estimation with adaptive arrays," *IEE Proc. F-Radar and Signal Process.*, vol. 140, no. 5, pp. 303-308, 1993.

[41] S. Han, A. De Maio, V. Carotenuto, L. Pallotta and X. Huang, "Censoring Outliers in Radar Data: An Approximate ML Approach and its Analysis," *IEEE Trans. Aerosp. Electron. Syst.*, vol. 55, no. 2, pp. 534-546, April 2019.

[42] S. D. Blunt and K. Gerlach, "Efficient robust AMF using the FRACTA algorithm," *IEEE Trans. Aerosp. Electron. Syst.*, vol. 41, no. 2, pp. 537-548, April 2005.

[43] P. Chen, W. L. Melvin, and M. Wicks, "Screening among multivariate normal data, " *J. Multivariate Anal.*, vol. 69, pp. 10-29, Apr. 1999.

[44] A. De Maio and M. Greco, Modern Radar Detection Theory. U.K.: The Institution of Engineering and Technology, 2015.

[45] E. J. Kelly, "An adaptive detection algorithm," *IEEE Trans. Aerosp. Electron. Syst.*, vol. 22, no. 1, pp. 115-127, 1986.

[46] F. C. Robey, D. R. Fuhrmann, E. J. Kelly, and R. Nitzberg, "A CFAR adaptive matched filter detector," *IEEE Trans. Aerosp. Electron. Syst.*, vol. 28, no. 1, pp. 208-216, 1992.

[47] R. S. Raghavan, N. Pulsone, and D. J. McLaughlin, "Performance of the GLRT for adaptive vector subspace detection," *IEEE Trans. Aerosp. Electron. Syst.*, vol. 32, no. 4, pp. 1473-1487, 1996.

[48] S. J. Wright, "Coordinate descent algorithms," *Mathematical Programming*, vol. 151, no. 1, pp. 3-34, 2015.

[49] B. Chen, S. He, Z. Li, and S. Zhang, "Maximum Block Improvement and Polynomial Optimization," *SIAM J. on Optimization*, vol. 22, no. 1, pp. 87-107, 2012.

[50] M. Razaviyayn, M. Hong, and Z. Luo, "A Unified Convergence Analysis of Block Successive Minimization Methods for Nonsmooth Optimization," *SIAM J. on Optimization*, vol. 23, no. 2, pp. 1126-1153, 2013.

[51] A. Aubry, A. De Maio, A. Zappone, M. Razaviyayn, and Z. Luo, "A New Sequential Optimization Procedure and Its Applications to Resource Allocation for Wireless Systems," *IEEE Trans. Signal Process.*, vol. 66, no. 24, pp. 6518-6533, 2018.

[52] L. M. Novak, M. C. Burl, and W. W. Irving, "Optimal polarimetric processing for enhanced target detection" *IEEE Trans. Aerosp. Electron. Syst.*, vol. 29, no. 1, pp. 234-244, 1993.

[53] A. De Maio, "Rao test for adaptive detection in Gaussian interference with unknown covariance matrix," *IEEE Trans. Signal Process.*, vol. 55, no. 7, pp. 3577-3584, 2007.

[54] S. M. Kay, Fundamentals of Statistical Signal Processing: Detection theory, Prentice Hall Signal Processing Series. Prentice-Hall PTR, 1998.

[55] E. Conte, A. De Maio, and C. Galdi, "Statistical analysis of real clutter at different range resolutions," *IEEE Trans. Aerosp. Electron. Syst.*, vol. 40, no. 3, pp. 903-918, July 2004.

[56] H. L. Van Trees, Optimum array processing: Part IV of detection, estimation, and modulation theory, Wiley-Interscience, 2002.

This article has been accepted for publication in IEEE Transactions on Aerospace and Electronic Systems. This is the author's version which has not been fully edited and content may change prior to final publication. Citation information: DOI 10.1109/TAES.2022.3210887

Lan Lan (S'19-M'20) was born in Xi'an, China in 1993. She received her B.S. degree in Electronic Engineering, and the Ph.D. degree in signal and information processing, both from Xidian University, Xi'an, China, in 2015 and 2020, respectively. She has been a visiting Ph. D student in the University of Naples Federico II, Naples, Italy, from July 2019 to July 2020. She is currently an Associated Professor at the National Laboratory of Radar Signal Processing, Xidian University. She was elected as the 'Youth Elite Scientist Sponsorship Program' by China Association for Science and Technology in 2022. She was a recipient of the Excellent Paper Award at the CIE 2016 International Conference on Radar. She is currently with the editorial boards of Digital Signal Processing.

Her research interests include frequency diverse array radar systems, MIMO radar signal processing, target detection, and ECCM.

Massimo Rosamilia (S'20) received the B.S. (with honors) and M.S. degrees in computer engineering from the University of Salerno, Fisciano, Italy, in 2017 and 2019, respectively. From September to November 2021, he was a Visiting Researcher with the Cranfield University, Shrivenham, U.K. He is currently working toward the Ph.D. degree in information technologies and electrical engineering with the University of Naples Federico II, Naples, Italy. His research interest lies in the field of statistical signal processing, with emphasis on radar signal processing. He ranked second in the Student Contest of the 1st International Virtual School on Radar Signal Processing, in 2020, with the contribution "Simultaneous Radar Detection and Constrained Target Angle Estimation via Dinkelbach Algorithm".

Augusto Aubry (M'12-SM'16) received the Dr. Eng. degree in telecommunication engineering (with honors) and the Ph.D. degree in electronic and telecommunication engineering both from the University of Naples Federico II, Naples, Italy, in 2007 and 2011, respectively. From February to April 2012, he was a Visiting Researcher with the Hong Kong Baptist University, Hong Kong. He is currently an assistant Professor with the University of Naples Federico II. His research interests include statistical signal processing and optimization theory, with emphasis on MIMO communications and radar signal processing. He is also the co-recipient of the 2013 Best Paper Award (entitled to B. Carlton) of the IEEE Transactions on Aerospace and Electronic Systems with the contribution "Knowledge-Aided (Potentially Cognitive) Transmit Signal and Receive Filter Design in Signal-Dependent Clutter".

Antonio De Maio (S'01-A'02-M'03-SM'07-F'13) received the Dr. Eng. (Hons.) and Ph.D. degrees in information engineering from the University of Naples Federico II, Naples, Italy, in 1998 and 2002, respectively. From October to December 2004, he was a Visiting Researcher with the U.S. Air Force Research Laboratory, Rome, NY, USA. From November to December 2007, he was a Visiting Researcher with the Chinese University of Hong Kong, Hong Kong. He is currently a Professor with the University of Naples Federico II. His research interest lies in the field of statistical signal processing, with emphasis on radar detection, optimization theory applied to radar signal processing, and multiple-access communications. He is the recipient of the 2010 IEEE Fred Nathanson Memorial Award as the young (less than 40 years of age) AESS Radar Engineer 2010 whose performance is particularly noteworthy as evidenced by contributions to the radar art over a period of several years, with the following citation for "robust CFAR detection, knowledge-based radar signal processing, and waveform design and diversity". He is the corecipient of the 2013 best paper award (entitled to B. Carlton) of the IEEE Transactions on Aerospace and Electronic Systems with the contribution "Knowledge-Aided (Potentially Cognitive) Transmit Signal and Receive Filter Design in Signal-Dependent Clutter".

Guisheng Liao (M'96-SM'16) was born in Guilin, Guangxi, China in 1963. He received his B.S. degree from Guangxi University, Guangxi, China, and M.S. and Ph.D. degrees from Xidian University, Xi'an, China, in 1985, 1990, and 1992, respectively. He is currently a Yangtze River Scholars Distinguished Professor at the NationalLaboratory of Radar Signal Processing and serves as Dean of the Hangzhou Institute of Technology, in Xidian University. Since 2009, He has been the evaluation expert for the international cooperation project of Ministry of Science and Technology in China. Since 2007, he has been the lead of Yangtze River Scholars Innovative Team and devoted in advanced techniques in signal and information processing. Since 2006, he has served as the panelists for the medium and long term development plan in high-resolution and remote sensing systems. From 1999 to 2000, He has been a Senior Visiting Scholar in the Chinese University of Hong Kong, Hong Kong.

His research interests include array signal processing, space-time adaptive processing, radar waveform design, and airborne/space surveillance and warning radar systems.

Jingwei Xu (M'15) was born in Shandong, China. He received the B.S. degree in electronic engineering, and the Ph.D. degree in signal and information processing, both from Xidian University, China, in 2010 and 2015, respectively. He is currently an Associated Professor at School of Electronic Engineering, Xidian University. From 2015 to 2017, he was a lecturer at National Lab of Radar Signal Processing in Xidian University. From 2017 to 2019, he was a Postdoctoral Fellow under "Hong Kong Scholar Program" at the City University of Hong Kong.

His research interests include radar system modeling, multi-sensor array signal processing, space-time adaptive processing, multiple-input multiple-output radar, and waveform diverse array radar.